Figure 2. Temporal kinetics of the behavioural aversion to light in mice. Graphs showing time spent in the dark back-half (BH) of the arena over the course of the 30-minute trial. Data are binned into 6, 5-minute bins throughout the trial, with y-axis showing average (±SEM) percentage time spent in the dark BH. (**A–D**) shows data from untreated animals, and (**E–H**) after bilateral application of atropine drops. (**A**) and (**E**) WT, (**B**) and (**F**) MO (*rd/rd cl*), (**C**) and (**G**) MKO (*Opn4*$^{-/-}$) and (**D**) and (**H**) TKO (*Opn4*$^{-/-}$ *Gnat1*$^{-/-}$ *Cnga3*$^{-/-}$). White triangles, trials when the front-half (FH) is in light, black triangles, trials when the FH is in darkness. Results of the regression analyses are shown in table 1. Stars (*) indicate significance levels (Bonferroni post tests, light FH v dark FH at each time point): * $p<0.05$; ** $p<0.01$; *** $p<0.001$.
doi:10.1371/journal.pone.0015009.g002

dark BH in the last 5 minutes. To compare the effect of the light to control conditions over the course of the trial, two–way repeated measures ANOVA (RM ANOVA) was carried out on data from each genotype, the results of Bonferroni post-tests are indicated on the graphs in Figure 2.

The WT (Figure 2A) and MO (Figure 2B) mice show a similar pattern of behaviour over the course of the trial, with the RM ANOVA test revealing a significant effect of time (WT $p<0.01$, MO $p<0.001$), light (WT $p<0.001$, $p<0.01$) and an interaction between time X light (WT $p<0.05$, MO $p<0.05$). In the last 5 minutes of the trial (minutes 25–30) the WTs and MOs spend the highest proportion of their time in the dark (87% WTs and 62% MOs). It is however clear when comparing the behaviour of WTs and MOs that melanopsin does not mediate all aspects of normal light aversion behaviour. Unlike MOs, the WT mice show a significant aversive response during the first 5 minutes of the trial and spend a higher proportion of their time in the dark BH.

As shown in Figure S2, aged MO animals retain their BLA, despite a well-documented loss of melanopsin cells with advancing age in these animals [51,52]. Interestingly, aging alters the behaviour of MO mice over the duration of the trial, so that during the first 5 minutes of the trial light aversion is intensified in older MOs compared to younger animals (Figure S2B). This result is of note and implies an increase in the potency of melanopsin signalling in retinal dystrophy with advancing age.

In MKO mice we found no significant correlation with duration of the trial and time spent in the dark BH. From the beginning to the end of the trial these mice spent 60% of their time in the back-half, similar to their overall average (Figure 2C). For this group of mice RM ANOVA showed a significant effect of light ($p<0.05$), but not for duration of trial or the interaction term light X time. As expected, the TKO mice did not display a significant aversion to light, with RM ANOVA showing no significant effect of light, time or the interaction term, with no differences between light FH and dark FH by Bonferroni post-tests. However, rather curiously, over the 30-minute trial duration, TKO mice do show a positive correlation with respect to the amount of time spent in the dark BH of the arena when the FH is illuminated (see Figure 2D and table 1).

In summary, when rods and cones are absent, melanopsin is capable of driving a slower onset BLA that is only clearly revealed after 15–20 minutes. Conversely, in the absence of melanopsin, animals retaining significant light aversion lack the positive correlation over time. Animals lacking melanopsin and properly functioning rods and cones (TKO) do not exhibit significant light aversion. Therefore, in order to display the aversion to light characteristic of their species, rodents must possess rods/cones and the photopigment melanopsin.

Ocular application of atropine enhances light aversion

In order to investigate the impact of eliminating the variable of pupillary constriction on BLA, atropine drops were applied

Table 1. Regression analysis of temporal kinetics of light aversion in mice.

Genotype	Treatment	Significant non-zero slope (p)	r^2	Slope
WT	Light Untreated	<0.05	0.68	1.05±0.36
WT	Dark Untreated	>0.05	-	-
MO	Light Untreated	<0.01	0.86	0.97±0.20
MO	Dark Untreated	>0.05	-	-
MKO	Light Untreated	>0.05	-	-
MKO	Dark Untreated	>0.05	-	-
TKO	Light Untreated	<0.05	0.75	0.56±0.16
TKO	Dark Untreated	>0.05	-	-
WT	Light Atropine	<0.05	0.78	1.01±0.27
WT	Dark Atropine	>0.05	-	-
MO	Light Atropine	<0.0001	0.99	1.46±0.07
MO	Dark Atropine	>0.05	-	-
MKO	Light Atropine	<0.01	0.87	0.88±0.17
MKO	Dark Atropine	>0.05	-	-
TKO	Light Atropine	<0.05	0.70	0.38±0.12
TKO	Dark Atropine	>0.05	-	-
TKO	Light Axotomy/Atropine	>0.05	-	-
TKO	Dark Axotomy/Atropine	>0.05	-	-
TKO	Light AAV2-ChR2V	<0.05	0.66	0.78±0.28

doi:10.1371/journal.pone.0015009.t001

bilaterally to the eyes 30 minutes prior to placing naïve animals into our open field arena. Other mydriatics were tested initially (e.g. phenylephrine, and tropicamide), however these agents were found to be either too short acting for the 30-minute trial and/or to cause mild distress, as such they were deemed unsuitable for use in combination with behavioural testing. Atropine on the other hand was ideal for this experiment as it relaxes the circular muscles of the iris to cause a painless and long-lasting mydriasis [53].

The application of atropine to the eyes of experimental animals produced no outward signs of discomfort and resulted in sustained pupil dilation. Figure 3A shows the PLR of MO mice to white light illumination (intensity-matched to that found in the experimental arena), following atropine application, the pupil no longer constricts. Unlike the other three genotypes tested here, TKO mice already lack pupil constriction, with neither atropine nor illumination able to change their pupil area (Figure 3B). It should be noted that the constriction mechanism itself in TKO mice remains intact, as demonstrated previously by application of the parasympathetic agonist carbachol [49].

As shown in Figure 1C, when atropine is applied prior to testing, all genotypes (including TKO mice) exhibit significant BLA, spending more time in the dark BH when the FH is illuminated. The influence of light and atropine in each genotype was assessed by two-way ANOVA followed by Bonferroni's multiple comparison tests. In the WT and MO there is a significant effect of light (WT, $p<0.001$; MO $p<0.001$) and atropine (WT, $p<0.001$; MO, $p<0.01$), there is also a significant interaction between light X atropine only in MO (WT, not significant; MO $p<0.05$). *Post hoc* tests reveal that with atropine application, light aversion is significantly increased ($p<0.01$) from 67% to 86% in WTs, and from 46% to 74% ($p<0.001$) in MOs. Atropine did not have a significant effect on behaviour in the dark in either the WTs or MOs.

Comparing the WT and MO behaviour by two-way ANOVA (factors: light and genotype) there is still an effect of both light ($p<0.0001$) and genotype ($p<0.05$) but by *post hoc* comparison testing the MO is no longer significantly less light aversive than the WT as was the case in the non atropine treated animals. Atropine application is therefore greatly enhancing melanopsin- mediated BLA, such that MOs lacking rods and cones are now behaving much more like WT animals. By contrast, in MKO mice atropine does not significantly enhance light aversion (Figure 2C), with two-way ANOVA revealing a significant effect of light ($p<0.01$) but not of atropine. In these animals, *post hoc* testing confirms there is no statistically significant change in light aversion with atropine application when either the FH is illuminated or in control conditions when the entire arena is in darkness.

Rather surprisingly, two-way ANOVA reveals a significant effect of atropine ($p<0.05$) and a significant interaction between light and atropine ($p<0.05$) in the TKO mice. *Post hoc* testing confirms that there is a significant increase in light aversion behaviour with the application of atropine ($p<0.01$) from 21% to 53% of time spent in the dark BH when the light is on. Again, atropine had no influence on behaviour in control conditions when the FH is in darkness.

Following atropine application, all the genotypes now show a positive correlation over the course of the trial spending more time in the dark BH as the trial progresses when the FH is illuminated

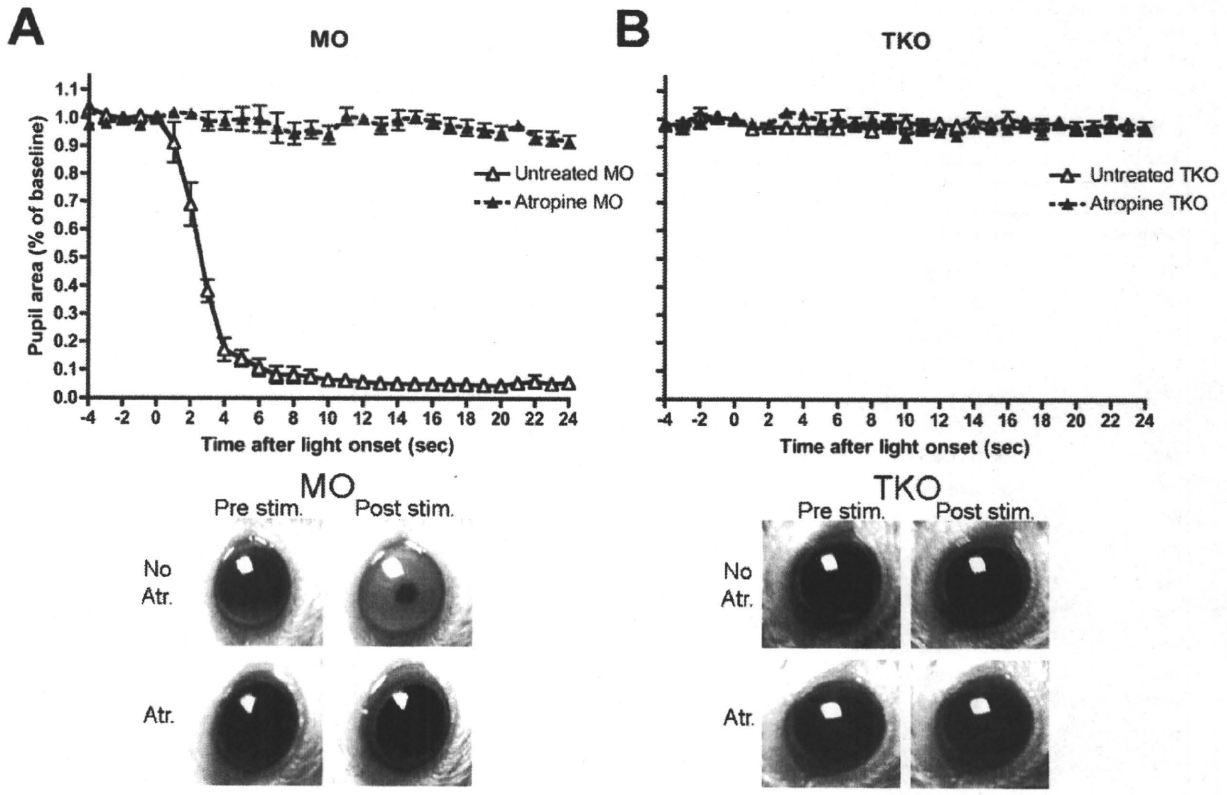

Figure 3. Effect of atropine on pupil size. In (**A**) MO (*rd/rd cl*), and (**B**) TKO (*Opn4*$^{-/-}$ *Gnat1*$^{-/-}$ *Cnga3*$^{-/-}$) mice. Images below each graph illustrate pupil size pre- and post- light stimulation with atropine (Atr.) or without atropine (No Atr.) application in the two genotypes.
doi:10.1371/journal.pone.0015009.g003

(Figure 2E–H; table 1). In the last 5 minutes of the light FH trial, WT mice spend 92% of the time in the dark BH, and at this point the MO is almost indistinguishable, spending 91% of the time in the dark. The MKO also spends most time in the dark at this point (76%), and surprisingly the TKO also exhibits quite a striking aversion to light, spending 60% of the time in the dark in the final 5 minutes of the trial. Two–way RM ANOVA of atropine treated WT (Figure 2E), MO (Figure 2F), and MKO (Figure 2G), behaviour reveals a significant effect of time (WT, $p<0.01$; MO, $p<0.0001$; MKO, $p<0.001$) light (WT, $p<0.001$; MO $p<0.001$; MKO, $p<0.001$) and an interaction between time X light (WT, $p<0.05$; MO, $p<0.01$; MKO $p<0.01$). The two-way RM ANOVA on atropine treated TKO mice (Figure 2H) shows there to be a significant effect of light ($p<0.05$) and a significant interaction between light X time ($p<0.05$) on BLA. It is clear that towards the end of the trial, TKO mice now spend significantly more time in the dark BH when the light is on in the FH than in control conditions with the dark FH.

The mechanism by which atropine is increasing light aversion in TKO mice is not readily apparent. In the other three genotypes (WT, MO and MKO), atropine application is causing pupil dilation and as such, their enhanced behavioural response could be attributed to more light entering the eye. However, in TKO mice this cannot be the case as we found their pupils to be fully dilated regardless of atropine administration (Figure 3B). As such, atropine would appear to be enhancing some residual light perception retained in these animals. This may be at the level of the retina or, alternatively, through a more systemic route acting on more central components of the visual system. Indeed, recent work from the Lucas laboratory has identified a small but significant electrophysiological response to light, both at the level of the ERG and the dorsal lateral geniculate nucleus of the thalamus [54]. To test the hypothesis that atropine might be influencing responsiveness of the TKO retina directly we carried out ERG recordings on these mice with and without atropine. Atropine does indeed significantly enhance the b-wave amplitude in TKO mice (Figure 4).

Aversion to light in TKO mice is driven by signals from the retina

In order to determine if the atropine-enhanced BLA of TKO mice was being driven by signals from the retina (as opposed to a local-systemic action of this drug on the brain), we used two complementary approaches: 1. Eliminate retinal input to the brain using bilateral axotomy and 2. Specifically render retinal neurons light sensitive using a non-pharmacological agent (the microbial opsin *Channelrhodopsin-2* (*ChR2*)), unable to potentiate the function of more remote components of the visual system.

For axotomy, in order to minimise the trauma associated with established procedures [55,56], we developed a novel technique that uses an intraocular, sub-retinal approach (see diagram in Figure 5A). As shown in Figure 5B and Figure S3, at 9 days post-axotomy, our technique has obliterated calretinin-positive retinal axons innervating the brain, confirming successful axotomy.

As shown in Figure 5C, after axotomy and subsequent atropine application, TKO mice no longer show a significant light aversion response over the whole trial (light FH versus dark FH Student's *t*-test $p>0.05$). Over the course of the trial there is also no correlation with the amount of time the animals spend in the dark BH with light FH or dark FH (see Figure 5D; Table 1). Also, Two-way RM ANOVA did not reveal any significant effects of light or trial duration on the time spent in the dark BH. These data show that axotomy abolishes the atropine-induced BLA in TKO mice.

In order to confirm that enhanced retinal output is sufficient to drive BLA in TKO mice, we rendered their retinae directly light sensitive. This was achieved by transfecting inner retinal neurons with *ChR2* using an intravitreal injection of an adeno-associated viral vector (AAV), which causes *Channelrhodopsin-2/Venus* (ChR2V) fusion protein expression in the retinal ganglion cells [57,58]. The expression of *ChR2V* gene is under the control of the CAG promoter which results in approximately 30% of retinal ganglion cells expressing *ChR2* [58]. It has previously been demonstrated that the viral construct we use here (AAV2-*ChR2V*) restores visual responses in rodents with degenerate rods/cones, while the Venus fluorescent reporter alone (AAV2-*Venus*) does not [57,58].

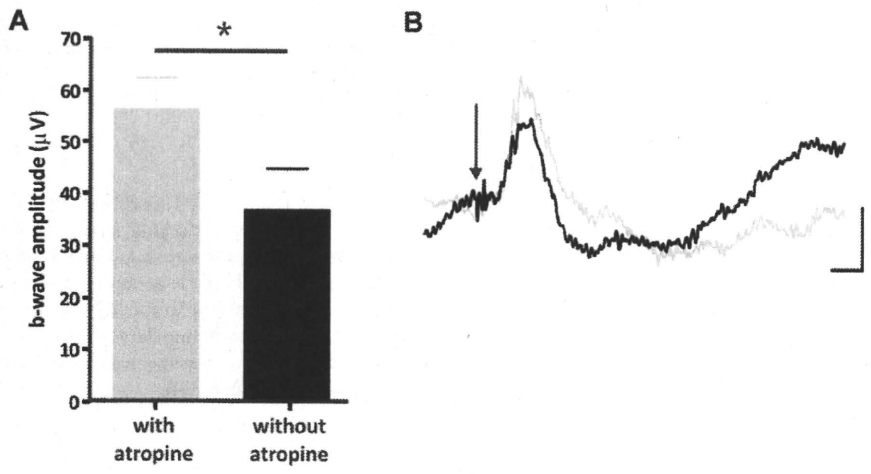

Figure 4. Atropine augments an ERG b-wave preserved in TKO mice. (**A**) b-wave amplitude of flash ERG responses in the presence and absence of atropine drops. A small but significant increase in the ERG b-wave amplitude was apparent following application of atropine drops (data presented as mean±SEM; n = 5 for each group). This is demonstrated in the average of all ERG responses in each group, shown in (**B**), atropine treated shown in grey, and untreated in black (scale bars: y-axis = 25 μV, x-axis = 50 ms; n = 5 for each group).
doi:10.1371/journal.pone.0015009.g004

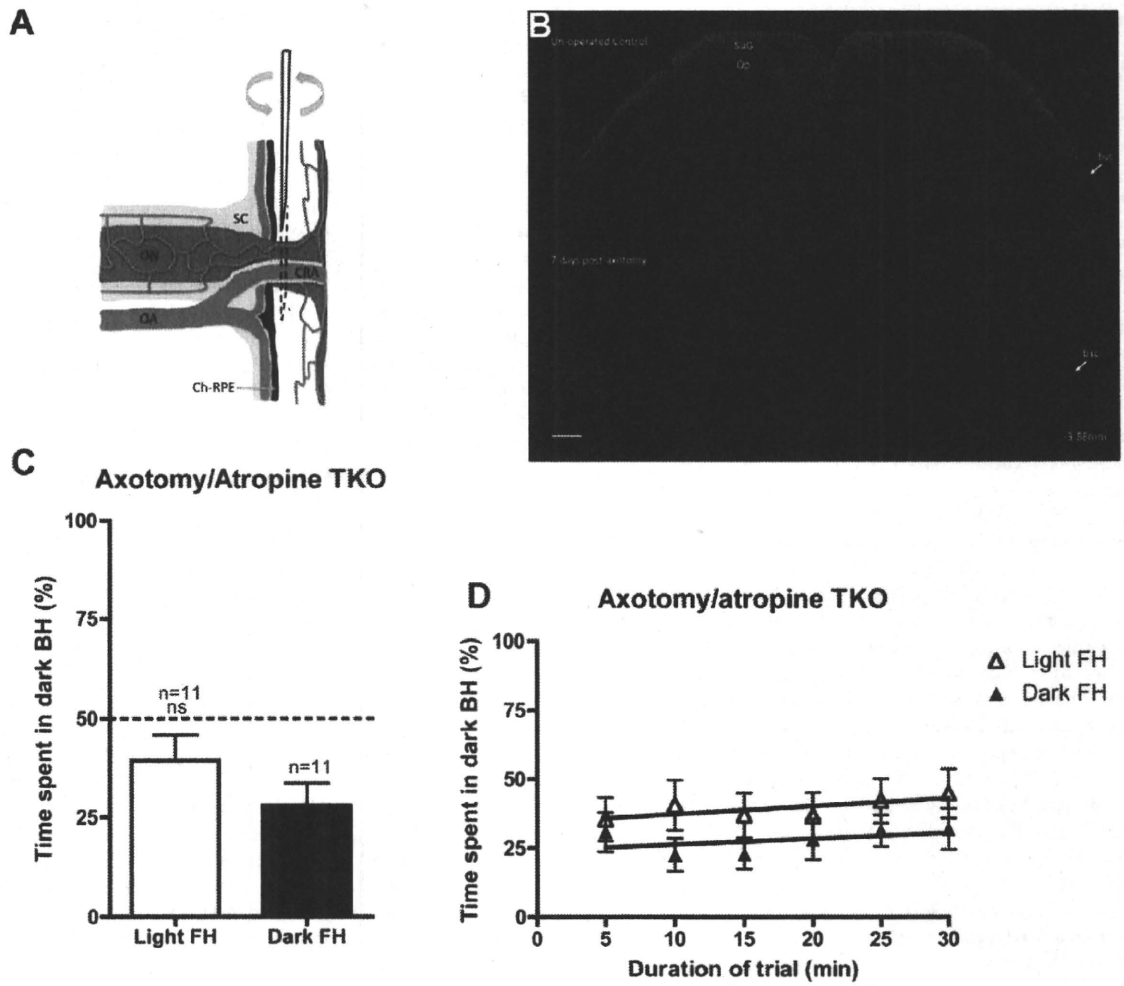

Figure 5. Axotomy abolishes the atropine-induced light aversion response in TKO mice. (**A**) Diagramatic illustration of the axotomy technique (image modified from [75]), a swift back and forth movement of the needle severs both the optic nerve and central retinal artery. (**B**) Immunoreactivity for calretinin positive retinal afferents (red) is abolished in the superficial gray (SuG) and the optic nerve (Op) layers of the superior colliculus of a bilaterally axotomised TKO (bottom) compared to an unoperated contol (top). Collicular sections are −3.88 mm from bregma [76], scale bar is 200 μm. (**C**) Behavioural aversion to light in atropine-treated TKO mice is abolished in bilaterally axotomised animals. (**D**) Time spent in the dark back half (BH) of the arena over the course of the 30-minute trial. White triangles, from trials when the front-half (FH) is in light, black triangles when the FH is in darkness. Abbreviations: bsc, brachium of the superior colliculus; Ch-RPE, choroid retinal pigment epithelium; CRA, central retinal artery; ns, not significant; OA, ophthalmic artery, ON, optic nerve; Sc, sclera.
doi:10.1371/journal.pone.0015009.g005

As shown in Figure 6, 2 months post-bilateral-injection of AAV2-*ChR2V* into adult TKO mice, cells across the entire inner retina were transduced to express ChR2V (green). In Figure 6B the red cells are stained for β-galactosidase, the reporter gene that replaces the melanopsin gene in TKO mice. Interestingly, by double-labelling in this fashion we very rarely encountered β-galactosidase positive cells that had been transduced to express the microbial opsin (<5 cells per retina).

As shown in Figure 6C, following ChR2V transduction, TKO mice (denoted AAV2-*ChR2V* TKO) now show an aversion to light similar to that of WT mice (WTs spend 67±4% (mean±SEM) and AAV2-*ChR2V* TKOs spend 68±10% (mean±SEM) in the dark back half when the front half is illuminated). The AAV2-*ChR2V* TKO mice also exhibit a positive correlation in their behaviour over the duration of the trial (Figure 6D), spending most time in the dark BH at the end of the trial (74%). Two-way RM ANOVA comparing the untreated to AAV2-*ChR2V* treated TKOs reveals a significant effect of treatment ($p<0.001$), and a significant effect of time ($p<0.05$). Bonferroni post tests show that at all time points during the trial, AAV2-*ChR2V* TKOs are significantly more averse to light than the untreated animals in the light (Figure 6D). Importantly for addressing the role of pupillary constriction in BLA, the transduced mice exhibited this strong aversion to light in the absence of a detectable PLR (Figure S4).

Discussion

The photopigment melanopsin has an established role in non-image forming behavioural responses to light such as circadian photoentrainment, negative masking and the induction of sleep [15,28,31,32,33]. It has also been shown to be sufficient for the acquisition of a Pavlovian association between light and

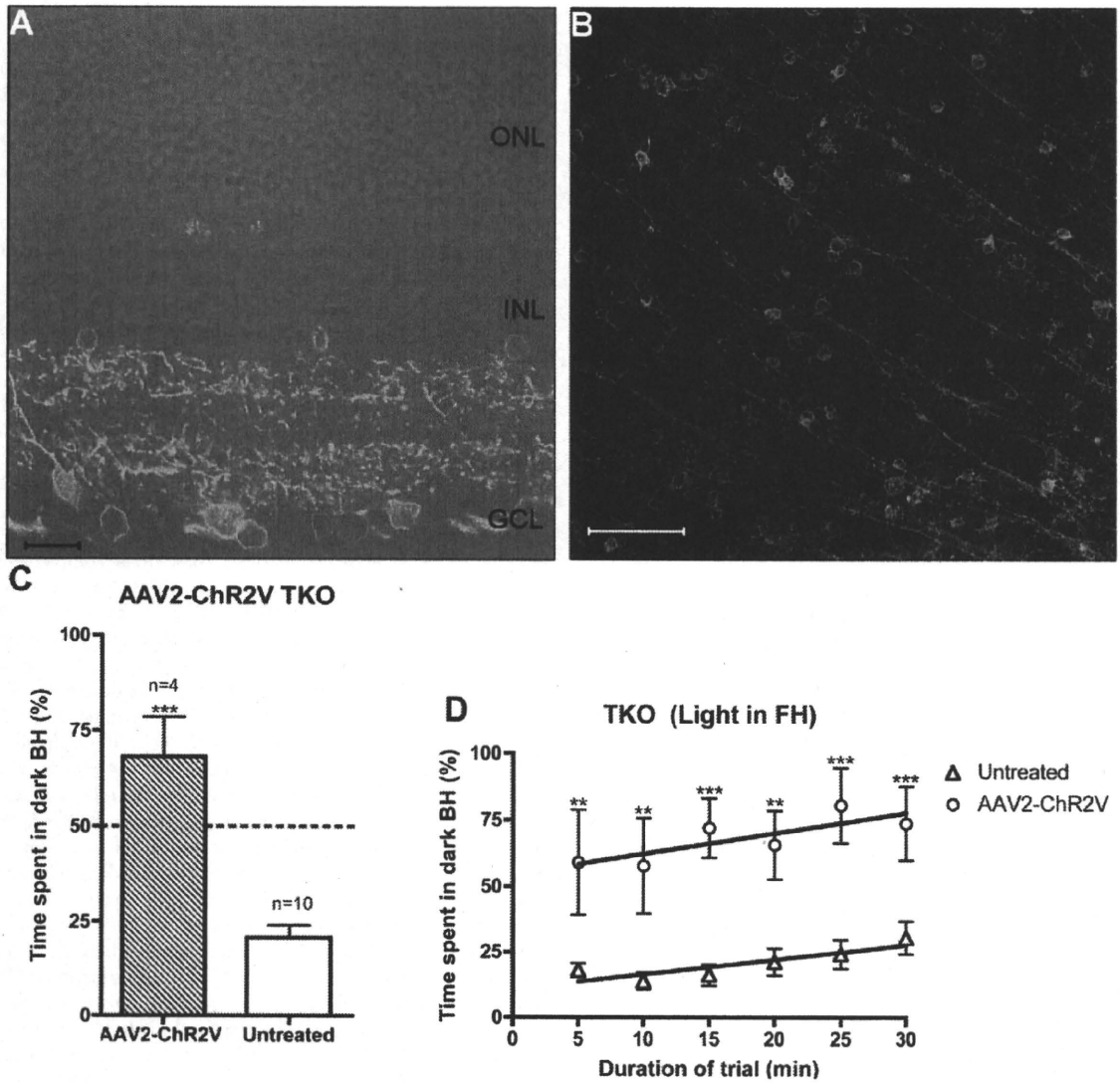

Figure 6. Channelrhodopsin-2 expression in the inner retina of TKO mice causes the induction of behavioural light aversion. (**A**) and (**B**) AAV2 transduced expression of Channelrhodopsin-2/Venus fusion (ChR2V) protein (green) in the ganglion cell layer of a TKO retina (AAV2-*ChR2V* TKO). (**A**) Transverse retinal section, ChR2V is visualised in many cells of the ganglion cell layer. Scale bar 20 μm (**B**) Immunohistochemistry on flat mount retina (focussing on the ganglion cell layer) for β-galactosidase (red) with ChR2V in green. Scale bar 100 μm. (**C–D**) Light aversion behaviour in the AAV2-*ChR2V* TKO. In these two graphs the comparison is between transduced and untreated animals when there is illumination in the front-half (FH). (**C**) Time spent in the dark back-half (BH) of the arena during the total 30 minutes of the trial. (**D**) Time spent in the dark (BH) of the arena over the course of the 30-minute trial. Stars (*) indicate significances (** $p<0.01$; *** $p<0.001$).
doi:10.1371/journal.pone.0015009.g006

impending negative reinforcement [34]. Here, using naïve adult mice, we confirm a new and important role for melanopsin in the attribution of emotional salience to light. Quite unexpectedly, our investigations also reveal a capacity for light perception/BLA in mice lacking three components deemed necessary for photoreception.

Melanopsin mediates a slow behavioural aversion to light

As reported for normally sighted animals in previous studies, we found a clear aversion to light by WT mice within the first 5 minutes of our test. However, in MO mice, where melanopsin alone drives this response there is a slower, more gradual BLA over time. The majority of light:dark testing paradigms used to date employ short trials (5–10 min duration) and we suggest that this may be one factor in the failure to report light aversion in previous studies using retinal degenerate rodents [19,20]. Our results are however consistent with those from a 22 h experiment suggesting a role for melanopsin in the preference displayed by *rd/rod*-ablated mice for a darkened nesting compartment [21]. Additionally, our data from MO mice shows that melanopsin-driven BLA has a strong positive correlation over time, potentiating light aversion over the course of our trial.

As with many other non-image forming responses to light, our data from MKO mice shows that melanopsin is not required for BLA to occur. However, these animals lack a positive correlation

over time, a result implicating melanopsin in the potentiation of outer retinal signalling as this behaviour progresses. We also found that older MO mice lose the positive correlation in BLA across time due to an enhanced light aversion in the first five minutes, an intriguing finding that suggests increased potency of melanopsin signalling with advancing age in retinal degeneration.

Although we have not examined BLA in neonatal animals here, the age (8–14 days old) at which rats were used in the initial studies by Crozier and Pincus [1] strongly implicates the involvement of the melanopsin system. This is because outer retinal function does not contribute to retinal activation prior to postnatal day 10 in mice [59] and between postnatal days 12–14 in rats [60].

An important component of our behavioural paradigm is the direct comparison between behaviour in light versus complete darkness. This method takes advantage of a phenomenon whereby, in the absence of light, animals will choose to spend the majority of a 30 minute period in the front half of the arena. The incorporation of this behaviour into our data analysis may help to explain why light aversion has not been reported previously over short durations in retinally degenerate rodents.

The light:dark choice test is regarded as an unconditioned conflict paradigm, where the innate tendency for light avoidance conflicts with the propensity of mice to explore/escape novel places into which they are forced [6,7]. To the best of our knowledge the robust behaviour in darkness we report has not previously been described. Although not easy to explain, we suggest this response may relate to an anxiety state which occurs in mice forced into a novel environment [61].

When mice are given the choice to freely explore something new they display a behaviour known as "neophobia" which involves initial retreat from and then progressive exploration of the novelty. If mice are presented simultaneously with a familiar and novel compartment to freely explore, they will spend approximately 75% of their time in the novel compartment. However, when they are forced into this novel compartment the animals display heightened anxiety levels, as measured by elevated corticosterone [61]. Thus, in the context of the present experiment, under complete darkness, a state of forced novelty exists. We suggest that in the absence of the aversive stimulus of light, mice may simply be returning to the point of entry which they associate with escape to the home cage.

In adult nocturnal rodents, BLA may contribute to diurnal behaviour by moving animals away from sunlight, towards darkened nesting areas where they would sleep. In this respect, the melanopsin-dependent temporal potentiation of BLA we identify here may be of particular importance in increasing motivation to leave open field environments. Given the role for melanopsin in modulating sleep [31,32,33] it will be important to examine the interaction between BLA and this other melanopsin-modulated behaviour in future experiments.

Although not available in the present study, it would be interesting to examine the performance of melanopsin aDTA mice [12,32] in our paradigm, these mice will help to determine the extent to which the mRGC pathway is required for BLA. However, like the MKO mice reported here, mice with a targeted destruction of mRGCs retain a behavioural aversion to light [18], indicating that mRGCs are probably not an absolute requirement for BLA.

Atropine application reveals a new element to light perception

Atropine pre-treatment led to a significant elevation of BLA in WT and MO mice, with both genotypes now responding to a similar level. The effect was particularly strong on the melanopsin component of BLA, strengthening the potentiation of this behaviour over time. In contrast, atropine failed to enhance the overall aversive response of MKO animals to light but did induce a positive correlation over time. We concluded from these experiments that BLA may normally be constrained by the PLR and that with fully dilated pupils, enhanced light stimulation of the retina increases the activity of outer and to a greater extent, inner retinal photoreceptors.

In order to control for the possibility that atropine may act independently of pupil dilation, we also added this drug to the eyes of TKO mice, which lack a PLR. To our complete surprise, this manipulation revealed an ability of TKOs to perceive light and display BLA. Previous work with these animals has shown that despite having an intact retina, they lack significant visual responsiveness [49]. Recent preliminary data indicates that TKO mice retain a small ERG with a spectral sensitivity matching rod opsin [54]. We report here that atropine application significantly enhances the b-wave component of this response and that bilateral axotomy abolishes the atropine-induced behavioural aversion to light exhibited by TKO mice. Thus, we suggest that atropine augments a residual retinal response in these animals, which is sufficient to drive BLA. In a complementary fashion, we confirm that in the absence of atropine, enhancing retinal light-responsiveness with ChR2 can also drive BLA in TKO mice in the absence of a PLR. The magnitude and temporal kinetics of this ChR2-mediated response are strikingly similar to BLA seen in WT mice, indicating that during development, the proximal neural circuitry for BLA can develop independently of normal rod, cone and melanopsin signalling. Interestingly, the behavioural effect in this experiment was achieved without significant transfection of mRGCs identified using β-galactosidase staining. Although this observation suggests that mRGCs may not be the only conduits mediating BLA, new evidence revealing an extended diversity of melanopsin expressing ganglion cells [36,62] raises the possibility that ChR2V may have been expressed in mRGCs that we could not detect.

During the preparation of this manuscript we became aware of another study examining the ability of phototransduction deficient MO mice ($Gnat1^{-/-}$, $Cnga3^{-/-}$) to perform pattern discrimination [36]. While these mice fail to respond to visual gratings in an optokinetic tracking test, in a forced-swim test, they can learn to use gratings of low spatial frequency to predict positive reinforcement (presence of an escape platform), while control TKOs ($Opn4^{-/-}$, $Gnat1^{-/-}$, $Cnga3^{-/-}$) cannot. This is accompanied by grating-induced c-Fos activation in primary visual cortex. The authors attribute these results solely to inner retinal melanopsin cells. Although no experimental data is presented, they also make the comment that control TKO mice retain an ability to discriminate between two screens in the visual learning task that vary significantly in luminance. This observation agrees with our findings of atropine-enhanced BLA and provides an independent account of light perception in TKO mice.

Interestingly, in another mouse model combining genetic ablation of rods with the disabling of cone phototransduction ($Rho^{-/-}$, $Cnga3^{-/-}$) there is no detectable ERG response [17]. This strongly implicates residual rod function in the retained visual capabilities of TKO mice, which have the same cone mutation ($Cnga3^{-/-}$) but possess structurally intact rods ($Gnat1^{-/-}$). This is in line with a previous report of atypical rod function under cone-isolating conditions [63] and cautions the use of genetic deactivation without cell death in order to isolate melanopsin function [32]. Indeed, it could be that because rods play an important role in rodent visual acuity within the photopic range [11], the melanopsin system may in fact be potentiating a rod-

driven signal to allow pattern discrimination by the visual system of mice lacking both *Gnat1*$^{-/-}$ and *Cnga3*$^{-/-}$ [36].

In terms of a mechanism of action for atropine in enhancing light-mediated BLA, it seems likely that there is a combination of pupillary dilation to spatially increase retinal luminance and a direct action on retinal signal processing. Interestingly, this information may be processed in the brain independently of established nociceptive pathways, as atropine, applied topically to the eyes fails to alter light-evoked responses in the spinal trigeminal nucleus [43]. In line with our findings, another recent study also reports that atropine (in combination with phenylepherine) can enhance ERG b-wave amplitudes in C57 wildtype and retinal degenerate mice [64]. The ability of atropine to enhance retinal function has implications for the interpretation of data arising from a range of visual neuroscience studies that employ this drug prior to measuring visual function [12,63,65].

Relevance of BLA in mice to human photophobia

Recently, the melanopsin system has been implicated in the circuitry by which light exacerbates the symptoms of migraine headache [42]. This study showed that patients with outer retinal degenerations consistently report migraine-associated photophobia. Using indirect evidence the authors propose a neural circuitry that involves information from mRGCs converging with trigemino-vascular signals in the lateral posterior thalamic nuclei before the integrated information is relayed up to cortical regions involved in pain processing.

Our results confirm that in retinal degenerate mice, melanopsin alone can drive a progressive behavioural aversion to light which is associated with activation of the visual and retrosplenial cortex. Both these structures are innervated to some extent by dura/light sensitive thalamic neurons [42]. In the context of behavioural aversion to light, our identification of melanopsin-driven c-Fos induction (Figure S1) in the retrosplenial cortex (RSC) is of particular interest because stimulation of this region in humans can cause autonomic responses linked to emotional processing [66]. The RSC is a posterior division of the cingulate cortex [67], a limbic structure which is active during the perception of photophobia in humans [44]. The established role of RSC in functions such as memory and navigation [68], together with its anatomical connectivity to structures such as the hippocampus and superior colliculus [69,70] make this an important structure to examine in future studies exploring melanopsin's role in emotional and cognitive processing, which are widely regarded to be interlinked [71].

Conclusions

Melanopsin in isolation is capable of attributing emotional salience to light sufficient to produce an aversive behavioural response that potentiates over time. This finding has relevance to the understanding of how spatial movements may be integrated with diurnal sleeping patterns to control circadian behaviour. Given the potential role for melanopsin in human photophobia, the study of brain regions involved in assigning affective valence to luminance represents an interesting avenue for future research. Surprisingly, the use of atropine to examine the role of the PLR in BLA also revealed that light perception, sufficient to generate an aversive behavioural response can occur in TKO mice, lacking melanopsin, a PLR and proper rod/cone function. The re-instatement of BLA in ChR2-transfected TKO mice confirms that pupillary constriction is not a requirement for light aversion in rodents.

Materials and Methods

Animals

All procedures were conducted according to the Home Office (UK) regulations, under the Animals (Scientific Procedures) Act of 1986, and with local (UCL-Institute of Ophthalmology, London, UK) ethics committee approval.

Four types of mice were used, wildtype (WT), *rd/rd cl* (melanopsin only, MO) [14,31], melanopsin knockout (MKO) *Opn4*$^{-/-}$ [30] and triple knockout (TKO) *Opn4*$^{-/-}$;*Gnat1*$^{-/-}$;*Cnga3*$^{-/-}$ [49]. The WT and MO are congenic on the C3H/He strain, whilst the MKO and TKO are a C57 BL6/129 mixed strain background. All animals were housed under a 12:12 light dark cycle, with food and water available *ad libitum*.

Pupillometry

The PLR was measured in un-anaesthetised mice dark adapted for at least 1 hour. An infra-red light source was used to illuminate the left eye and frames were taken using a 12 bit SMD (1M60) digital camera mounted on top of a Leica MZ75 microscope using a magnification of 1. A long pass filter was interposed between the microscope lens and the mouse eye to block any light of less than 665 nm wavelength. The left eye was stimulated with broad-spectrum light originating from a xenon-arc lamp (Lambda DG-4, Linton Instrumentation) synchronized with the image capture using an electronic shutter (Melles-Griot). Short-pass and neutral density filters (Edmund Optics Ltd., York, UK) were combined to abolish stimulus light wavelengths above 600 nm. The light was then guided with a fibre optic through a light diffuser placed 2 cm away from the left eye stimulating with white light of 600 $\mu W/cm^2$ irradiance. The eye was stimulated for 24 seconds while collecting spatially binned (2×2) frames of the eye at 4 Hz. The pupil area was estimated off-line at each frame by an observer using customized MATLAB software and the results were downsampled to 1 Hz. Pupillometry was carried out on n = 5 TKO, n = 3 MO, and n = 4 TKO mice treated with AAV-*ChR2V*. One day after PLR assessment of the TKO and MO the same mice had bilateral application of atropine sulphate, 1%, (Minims, preservative free) under dim red light. After 1 hour of dark adaptation recording of their PLR was made as described above.

Testing of open field light aversion behaviour

Adult mice (~100–250 days of age) of mixed sexes were used. We chose to use mice naïve to the experimental arena because although habituation is used in some light/dark choice protocols [72] this can reduce the amount of time spent in the dark [73] which may mask subtle light responses. The open field arena is shown in Figure 1A. The arena is square (26×26 cm) and is divided in half into an open front-half (FH) and an enclosed back-half (BH), with a small door through which the mouse can enter the enclosed area. The FH of the arena was either illuminated (light FH) or remained in darkness (dark FH) with a light-impervious cloth used to baffle the arena from stray sources of light. White light illumination was provided by a Philips Energy Light (Philips, Guildford UK) suspended 0.75 m above the whole arena (irradiance at floor level 600 $\mu W/cm^2$ or ~1300 Lux). The illumination did not cause a measurable change in temperature in the FH of the arena compared to the BH, as measured using heat probes. Air conditioning in the room served to regulate the temperature and also produced background white noise.

Only naïve animals were tested, that did not have previous exposure to the arena. All tests were carried out during the light phase (ZT1-11) of their light:dark cycle, and all animals were light adapted. At the start of each trial, each mouse was placed in the

FH of the arena under dim red illumination (after which this red light was turned off) and left for 30 minutes with either illumination or darkness in the FH. The time spent in each compartment was monitored using TRUSCAN (Coulburn Instruments, Inc Allentown, PA). After each trial the arena was thoroughly washed and then wiped with 70% ethanol and dried.

Some animals were treated with atropine prior to being tested in the arena. Here, animals were taken from their holding room, to a separate procedure room where 1 drop of atropine sulphate, 1%, (Minims, preservative free) was applied bilaterally, and the animals were then left in their home cage for at least 0.5–2 hours prior to being tested in a separate procedure room containing the open field arena.

Animals that did not enter the BH of the arena within the first 5 minutes of a trial were discounted from the analysis. Total numbers tested and those discounted are shown in table S1. In general, most animals entered the BH within the first couple of minutes and, in terms of latency to enter the BH, no significant differences between the genotypes or between different illuminations (light vs. darkness) were found (data not shown).

Bilateral intraocular axotomy procedure

For axotomy surgery, triple knockout mice were deeply anaesthetized with a mixture of medetomidine hydrochloride (1 mg/kg) (Domitor, Pfizer, Kent, UK) and ketamine (75 mg/kg) and placed securely in a nose bar with eyes covered in ViscoTears (Novartis Pharmaceuticals UK Ltd). An ophthalmic operating microscope (Olympus) was used to visualize the optic nerve head directly through a glass coverslip before gripping the extra-ocular muscles with a pair of fine-toothed microsurgical tweezers (FST) and inserting a 30-gauge needle (attached to a 2.5 µl Hamilton syringe) through the sclera, directly into the sub-retinal space. This technique uses the same needle and sub-retinal approach that is routinely employed in cell transplantation studies [74]. Once the needle was sub-retinal and adjacent to the optic nerve head, the optic nerve (together with the central retinal artery) was easily severed using a swift back and forth movement. This surgical procedure is summarized in Figure 5A (in a schematic adapted from May and Lutjen-Drecoll, 2002 [75]). At the time of surgery, axotomy was confirmed by injecting 2 µl of saline to produce a retinal detachment beneath the successfully severed optic nerve head.

Following bilateral axotomy surgery, all animals were given an intra-peritoneal injection of the analgesic carprofen 5 mg/kg (Rimadyl, Pfizer, Kent, UK) and recovered with the anaesthetic antidote atipamezole 0.5 mg/kg (Anti-sedan Pfizer, Kent, UK). Animals had recovered well by the following morning and were run in the light aversion assay 8 days post-surgery. One day following the completion of behavioural testing, all mice were perfused and their brains processed for calretinin immunohistochemistry. In addition to the axotomised mice, for the purposes of comparison, several age-matched untreated TKOs (n = 3) were also perfused and their brains processed for calretinin immunohistochemistry. The anatomical positioning of brain sections was determined using the mouse brain atlas [76]. The calcium binding protein calretinin is expressed ubiquitously in retinal ganglion cell axons and is a well-characterised marker for assessing deafferentation of subcortical retino-recipient structures in the rodent [77]. Previous work in the rat [78] and mouse [79] has demonstrated that calretinin-positive axonal fibres in the superficial layers of superior colliculus originate exclusively from retinal ganglion cells and that these fibres are lost 7 days following successful optic nerve section.

AAV vector injection

The preparation of the adeno-associated viral (AAV) vector used here has been described in detail previously [57]. In brief, it contains a *Channelrhodopsin-2/Venus* (*ChR2V*) fusion gene under the control of a hybrid cytomegalovirus/chicken β actin promoter. Four TKO adult mice (162 day-old) underwent bilateral intravitreal injections of the AAV2-*ChR2V* viral vector suspension (1×10^{12} particles/ml, measured by an ELISA assay as described previously [80]).

Mice were anaesthetised as above and the head stabilised in a nose-bar before inserting a 30-gauge needle (attached to a 2.5 µl Hamilton syringe) into the vitreous cavity. A total volume of 2 µl of the viral vector suspension was injected into each eye, followed by a parasentesis counter-injection made below the *ora serrata* (to relieve intraocular pressure). The mice were recovered as described above and tested two-months post-surgery for photophobic behaviour and pupillometry. Finally, they were perfused and the eyes processed for immunohistochemistry, with one retina from each animal removed and processed as a flat mount whilst the other was cryprotected, frozen and sectioned.

Electroretinogram recordings

Experimentation was performed under dim red light (<0.25 µW/cm^2, >650 nm), and mice were long-term dark adapted (>12 hr) prior to recording. To compare the effects of atropine on the TKO ERG, mice were divided into two groups: 5 mice received atropine sulphate eye drops (1%; minims, preservative free) in each eye 30 minutes prior to recording, and 5 mice received no drops. Mice were initially anaesthetised with intra-peritoneal ketamine (70 mg/kg) and xylazine (7 mg/kg), which was maintained with an injection of subcutaneous ketamine (72 mg/ml) and xylazine (5 mg/ml).

Hypromellose solution (0.5%; Alcon Laboratories, Ltd., UK) was applied to each eye to retain corneal moisture and to provide sufficient adherence of a contact lens electrode to the corneal surface. A silver wire bite bar provided head support and acted as a ground, and a needle reference electrode (Ambu® Neuroline) was inserted approximately 5 mm from the base of contralateral eye, sufficiently distal to exclude signal interference. Electrodes were connected to a Windows PC via a signal conditioner (Model 1902 Mark III, CED, UK), which differentially amplified (x3000) and filtered (band-pass filter cut-off 0.5 to 200 Hz) the signal, and a digitizer (Model 1401, CED). Throughout experimentation, core body temperature was maintained at ~37°C via a homeothermic heat mat (Harvard Apparatus, Kent, UK). For ten minutes prior to first recordings, electrode stability was monitored; electrodes displaying any baseline instability were rejected.

A xenon arc source (Cairn Research Ltd., Kent, UK) connected to a ganzfeld sphere provided white light flashes with a peak corneal irradiance of 1.58 mW/cm^2 (2370 Lux). A series of 15 ms flashes were applied using an electrically controlled mechanical shutter (Cairn Research Ltd.) with a 40 s interstimulus interval. An average ERG response was generated from 25 flashes, and the b-wave amplitude measured (from a-wave peak to b-wave peak) and compared statistically.

Immunohistochemistry

Animals were deeply anaesthetised with sodium pentobarbital (60 mg/kg) and then perfused with 0.1 M PBS followed by 4% paraformaldehyde (in 0.1 M phosphate buffer), with overnight post-fixation at 4°C. Tissues to be cryostat sectioned were cryoprotected overnight at 4°C in 30% sucrose solution (in 0.1 M PBS), and then frozen with a dry ice/acetone slurry. Coronal brain sections (30 µm thick) were cut on the cryostat and

processed free-floating, while retinal sections were cryosectioned (14 μm thick) and mounted onto Superfrost Plus slides (BDH, Poole, UK).

Tissues were blocked for 2 h with 5% normal donkey serum (NDS) in PBS containing 0.3% (retinal/brain sections) or 3% (flat mounts) Triton X-100 (PBS-TX). The tissue was subsequently incubated overnight in PBS-TX containing 1% NDS and either a goat primary antibody raised against calretinin (1:1000, Swant, Bellinzona, Switzerland) or a rabbit anti-β galactosidase antibody (1:5,000, Abcam, Cambridge, UK). Following washes in PBS, tissue was incubated for 2 h in PBS-TX containing 2% NDS and an appropriate TRITC-labelled secondary antibody (1:200, Jackson ImmunoReseach, West Grove, PA). Tissue was washed extensively in PBS and TRIS buffer. Cell nuclei were counterstained with DAPI (1:5,000 Sigma) before cover-slipping with Vectashield (Vector Laboratories, Burlingame, CA). Fluorescence labelling was examined using a Zeiss confocal microscope (with LSM Image Browser software, Welwyn Garden City, UK).

Statistical Analysis

All data was analysed using GraphPad Prism software (GraphPad Software, San Diego, CA). Prior to analysis by Student's *t*-tests or ANOVA the proportional light aversion data were transformed Y = Arcsine(Y). One-tailed Student's *t*-tests were used to analyse both the effect of light on the total amount of time spent in the dark BH (light FH versus dark FH) over the whole 30-minute trial, and also the electroretinogram b-wave data. To analyse the effect of rods and cones, light aversion behaviour was compared between the congenic WT and MO by two-way ANOVA (factors: genotype and light) followed by Bonferroni's multiple comparison tests. To analyse the effect of atropine a two-way ANOVA (factors: light and atropine) was performed followed by Bonferroni's multiple comparison tests. The effect of light over the duration of the trial was investigated by using both regression analysis and two-way repeated measures ANOVA (RM ANOVA), factors: light and duration of the trial, (subjects were significantly matched in all cases $p<0.0001$) this was followed by Bonferroni post-tests with light FH versus dark FH at each time point in the trial.

Supporting Information

Figure S1 Light induced c-fos in the visual and retrosplenial cortex (RSC) of MO (*rd/rd cl*) mice. Images on the left are from an animal that remained in the dark whilst those on the right from an animal that was exposed to light. Nuclei positive for the immediate early gene c-Fos are green, whilst neurofilament-H (NF-H) is in red. (**A**) Montage of the cortex, −3.52 mm from the Bregma, Scale bar 400 μm. (**B**) Higher magnification of the medial visual cortex (V1/2) clearly showing light induced neural activity in layers II–VI. (**C**) Higher magnification of the retroplenial cortex showing light induced c-Fos, (**B–C**) Scale bars 200 μm. Methods: Mice (n = 3 per condition) were dark-adapted overnight and at 07:00, still in their home cages, either exposed to 1.5 hours of ~1300 lux white light or maintained in darkness. They were then perfused and brain sections processed for immunohistochemistry as described in the main text using rabbit anti-c-fos (PC38, Calbiochem, 1:5,000) and mouse anti-neurofilament heavy chain (SMI-32, Covance, 1:5,000) followed by secondaries antibodies (FITC anti-rabbit IgG and TRITC anti-mouse IgG, both from Jackson ImmunoReseach, West Grove, PA). The neurofilament-H antibody was used to match up sections using cytoarchitectural boundaries in the cortex, as described previously by Van der Gucht *et al.*, 2007. (TIF)

Figure S2 Behavioural light aversion in old versus young MO (*rd/rd cl*) mice. (**A**) The amount of time old animals (394±46 day-old; mean±SD) spend in the dark back-half (BH) during the 30-min trial is not significantly different to the amount of time spent there by younger animals (166±6 day-old), although the average time that the old animals spend in the dark is slightly higher (~58% versus ~46%). (**B**) Over the course of the trial it is revealed that the old animals spend significantly more time (~70%) in the dark than the younger animals during the first 5 minutes of the trial (Two-way repeated measures ANOVA demonstrates: (1) a significant interaction ($p<0.05$) aging X duration of the trial and (2) a significant effect of duration ($p<0.05$), Bonferonni post-tests show that in the first 5 minutes the old animals spend significantly more time in the dark ($p<0.01$) than younger animals). It seems unlikely that this is due to poorer mobility in the old animals as they continued to move around the arena sampling both light and dark regions for the rest of the trial. Due to this behaviour during the first 5-minutes there is no longer a significant positive correlation of photophobic behaviour in the old animals, they continue spending a similar proportion of their time in the dark BH throughout the 30 minutes. Abbreviations: BH, back-half; MO, melanopsin only. (TIF)

Figure S3 Calretinin positive retinal-afferents (red) are lost 9 days post axotomy in the olivary pretectal nucleus (OPT) and the optic chiasm (och) of TKO mice. Compare **A** with **B** for the OPT and **C** with **D** for the och. Brain sections from equivalent Bregma positions were imaged in control and axotomised brains as indicated in **A** for the OPT and in **C** for the och. Scale bar in D for all plates is 100 μm. Abbreviations: oc, optic chiasm; OPT, olivary pretectal nucleus; TKO, triple knockout. (TIF)

Figure S4 Pupillometry in triple knockout (TKO) mice following transduction of the inner retina with Channelrhodopsin 2/Venus fusion protein. At two-months post-introduction of the AAV2-*ChR2V* the pupillary light reflex has not been re-instated in these animals. (TIF)

Table S1 (DOC)

Acknowledgments

We gratefully acknowledge the kind help and assistance of Prof. Rob Lucas from the University of Manchester. We also thank Prof. Russell G. Foster of Oxford University for providing *rd/rd cl* mice. We wish to acknowledge the technical assistance of Matthew Smart and Shazeen Hasan.

Author Contributions

Conceived and designed the experiments: MS PJC AAV. Performed the experiments: MS CG AA AEA JML AAV. Analyzed the data: MS CG AEA. Contributed reagents/materials/analysis tools: ES HT. Wrote the paper: AAV MS.

References

1. Crozier WJ, Pincus G (1927) Phototropism in Young Rats. J Gen Physiol 10: 407–417.
2. Keller FS (1941) Light aversion in the white rat. Psychological Record 4: 235–250.
3. Welker WI (1959) Escape, exploratory, and food-seeking responses of rats in a novel situation. J Comp Physiol Psychol 52: 106–111.
4. Flynn JP, Jerome EA (1952) Learning in an automatic multiple-choice box with light as incentive. J Comp Physiol Psychol 45: 336–340.

5. Crawley J, Goodwin FK (1980) Preliminary report of a simple animal behavior model for the anxiolytic effects of benzodiazepines. Pharmacol Biochem Behav 13: 167–170.
6. Misslin R, Belzung C, Vogel E (1989) Behavioural validation of a light/dark choice proceedure for testing anti-anxiety agents. Behavioural Process 18: 119–132.
7. Bourin M, Hascoet M (2003) The mouse light/dark box test. Eur J Pharmacol 463: 55–65.
8. Recober A, Kaiser EA, Kuburas A, Russo AF (2010) Induction of multiple photophobic behaviors in a transgenic mouse sensitized to CGRP. Neuropharmacology 58: 156–165.
9. Russo AF, Kuburas A, Kaiser EA, Raddant AC, Recober A (2009) A Potential Preclinical Migraine Model: CGRP-Sensitized Mice. Mol Cell Pharmacol 1: 264–270.
10. Altman J (1962) Effects of lesions in central nervous visual structures on light aversion of rats. Am J Physiol 202: 1208–1210.
11. Schmucker C, Seeliger M, Humphries P, Biel M, Schaeffel F (2005) Grating acuity at different luminances in wild-type mice and in mice lacking rod or cone function. Invest Ophthalmol Vis Sci 46: 398–407.
12. Guler AD, Ecker JL, Lall GS, Haq S, Altimus CM, et al. (2008) Melanopsin cells are the principal conduits for rod-cone input to non-image-forming vision. Nature 453: 102–105.
13. Provencio I, Rollag MD, Castrucci AM (2002) Photoreceptive net in the mammalian retina. This mesh of cells may explain how some blind mice can still tell day from night. Nature 415: 493.
14. Lucas RJ, Freedman MS, Munoz M, Garcia-Fernandez JM, Foster RG (1999) Regulation of the mammalian pineal by non-rod, non-cone, ocular photoreceptors. Science 284: 505–507.
15. Freedman MS, Lucas RJ, Soni B, von Schantz M, Munoz M, et al. (1999) Regulation of mammalian circadian behavior by non-rod, non-cone, ocular photoreceptors. Science 284: 502–504.
16. Berson DM, Dunn FA, Takao M (2002) Phototransduction by retinal ganglion cells that set the circadian clock. Science 295: 1070–1073.
17. Barnard AR, Appleford JM, Sekaran S, Chinthapalli K, Jenkins A, et al. (2004) Residual photosensitivity in mice lacking both rod opsin and cone photoreceptor cyclic nucleotide gated channel 3 alpha subunit. Vis Neurosci 21: 675–683.
18. Goz D, Studholme K, Lappi DA, Rollag MD, Provencio I, et al. (2008) Targeted destruction of photosensitive retinal ganglion cells with a saporin conjugate alters the effects of light on mouse circadian rhythms. PLoS ONE 3: e3153.
19. Hetherington L, Benn M, Coffey PJ, Lund RD (2000) Sensory capacity of the royal college of surgeons rat. Invest Ophthalmol Vis Sci 41: 3979–3983.
20. Lin B, Koizumi A, Tanaka N, Panda S, Masland RH (2008) Restoration of visual function in retinal degeneration mice by ectopic expression of melanopsin. Proc Natl Acad Sci U S A 105: 16009–16014.
21. Mrosovsky N, Hampton RR (1997) Spatial responses to light in mice with severe retinal degeneration. Neurosci Lett 222: 204–206.
22. Jimenez AJ, Garcia-Fernandez JM, Gonzalez B, Foster RG (1996) The spatio-temporal pattern of photoreceptor degeneration in the aged rd/rd mouse retina. Cell Tissue Res 284: 193–202.
23. Garcia-Fernandez JM, Jimenez AJ, Foster RG (1995) The persistence of cone photoreceptors within the dorsal retina of aged retinally degenerate mice (rd/rd): implications for circadian organization. Neurosci Lett 187: 33–36.
24. Punzo C, Kornacker K, Cepko CL (2009) Stimulation of the insulin/mTOR pathway delays cone death in a mouse model of retinitis pigmentosa. Nat Neurosci 12: 44–52.
25. Lin B, Masland RH, Strettoi E (2009) Remodeling of cone photoreceptor cells after rod degeneration in rd mice. Exp Eye Res 88: 589–599.
26. Isoldi MC, Rollag MD, Castrucci AM, Provencio I (2005) Rhabdomeric phototransduction initiated by the vertebrate photopigment melanopsin. Proc Natl Acad Sci U S A 102: 1217–1221.
27. Panda S, Nayak SK, Campo B, Walker JR, Hogenesch JB, et al. (2005) Illumination of the melanopsin signaling pathway. Science 307: 600–604.
28. Mrosovsky N, Lucas RJ, Foster RG (2001) Persistence of masking responses to light in mice lacking rods and cones. J Biol Rhythms 16: 585–588.
29. Lucas RJ, Douglas RH, Foster RG (2001) Characterization of an ocular photopigment capable of driving pupillary constriction in mice. Nat Neurosci 4: 621–626.
30. Lucas RJ, Hattar S, Takao M, Berson DM, Foster RG, et al. (2003) Diminished pupillary light reflex at high irradiances in melanopsin-knockout mice. Science 299: 245–247.
31. Lupi D, Oster H, Thompson S, Foster RG (2008) The acute light-induction of sleep is mediated by OPN4-based photoreception. Nat Neurosci 11: 1068–73.
32. Altimus CM, Guler AD, Villa KL, McNeill DS, Legates TA, et al. (2008) Rods-cones and melanopsin detect light and dark to modulate sleep independent of image formation. Proc Natl Acad Sci U S A 105: 19998–20003.
33. Tsai JW, Hannibal J, Hagiwara G, Colas D, Ruppert E, et al. (2009) Melanopsin as a sleep modulator: circadian gating of the direct effects of light on sleep and altered sleep homeostasis in Opn4(−/−) mice. PLoS Biol 7: e1000125.
34. Mrosovsky N, Salmon PA (2002) Learned arbitrary responses to light in mice without rods or cones. Naturwissenschaften 89: 525–527.
35. Hattar S, Kumar M, Park A, Tong P, Tung J, et al. (2006) Central projections of melanopsin-expressing retinal ganglion cells in the mouse. J Comp Neurol 497: 326–349.
36. Ecker JL, Dumitrescu ON, Wong KY, Alam NM, Chen SK, et al. (2010) Melanopsin-Expressing Retinal Ganglion-Cell Photoreceptors: Cellular Diversity and Role in Pattern Vision. Neuron 67: 49–60.
37. Dacey DM, Liao HW, Peterson BB, Robinson FR, Smith VC, et al. (2005) Melanopsin-expressing ganglion cells in primate retina signal colour and irradiance and project to the LGN. Nature 433: 749–754.
38. Zaidi FH, Hull JT, Peirson SN, Wulff K, Aeschbach D, et al. (2007) Short-wavelength light sensitivity of circadian, pupillary, and visual awareness in humans lacking an outer retina. Curr Biol 17: 2122–2128.
39. Drummond PD (1986) A quantitative assessment of photophobia in migraine and tension headache. Headache 26: 465–469.
40. Lebensohn J (1934) The nature of photophobia. Archives of Ophthalmology 12: 380–390.
41. Lebensohn JE (1951) Photophobia: mechanism and implications. Am J Ophthalmol 34: 1294–1300.
42. Noseda R, Kainz V, Jakubowski M, Gooley JJ, Saper CB, et al. (2010) A neural mechanism for exacerbation of headache by light. Nat Neurosci 13: 239–245.
43. Okamoto K, Tashiro A, Chang Z, Bereiter DA (2010) Bright light activates a trigeminal nociceptive pathway. Pain 149: 235–242.
44. Moulton EA, Becerra L, Borsook D (2009) An fMRI case report of photophobia: activation of the trigeminal nociceptive pathway. Pain 145: 358–363.
45. King V (1972) Discomfort glare from flashing sources. J Am Optom Assoc 43: 53–56.
46. Stringham JM, Fuld K, Wenzel AJ (2004) Spatial properties of photophobia. Invest Ophthalmol Vis Sci 45: 3838–3848.
47. Sliney DH (1997) Ocular exposure to environmental light and ultraviolet—the impact of lid opening and sky conditions. Dev Ophthalmol 27: 63–75.
48. Stringham JM, Fuld K, Wenzel AJ (2003) Action spectrum for photophobia. J Opt Soc Am A Opt Image Sci Vis 20: 1852–1858.
49. Hattar S, Lucas RJ, Mrosovsky N, Thompson S, Douglas RH, et al. (2003) Melanopsin and rod-cone photoreceptive systems account for all major accessory visual functions in mice. Nature 424: 76–81.
50. Van der Gucht E, Hof PR, Van Brussel L, Burnat K, Arckens L (2007) Neurofilament protein and neuronal activity markers define regional architectonic parcellation in the mouse visual cortex. Cereb Cortex 17: 2805–2819.
51. Semo M, Lupi D, Peirson SN, Butler JN, Foster RG (2003) Light-induced c-fos in melanopsin retinal ganglion cells of young and aged rodless/coneless (rd/rd cl) mice. Eur J Neurosci 18: 3007–3017.
52. Semo M, Peirson S, Lupi D, Lucas RJ, Jeffery G, et al. (2003) Melanopsin retinal ganglion cells and the maintenance of circadian and pupillary responses to light in aged rodless/coneless (rd/rd cl) mice. Eur J Neurosci 17: 1793–1801.
53. Reader AL, 3rd (1977) Mydriasis from Datura wrightii. Am J Ophthalmol 84: 263–264.
54. Allen AE, Cameron MA, Brown TM, Vugler AA, Lucas RJ (2010) Visual responses in mice lacking critical components of all known retinal phototransduction cascades. PLoS ONE 10.1371/journal.pone.0015063.
55. Lau KC, So KF, Campbell G, Lieberman AR (1992) Pupillary constriction in response to light in rodents, which does not depend on central neural pathways. J Neurol Sci 113: 70–79.
56. Robinson GA, Madison RD (2004) Axotomized mouse retinal ganglion cells containing melanopsin show enhanced survival, but not enhanced axon regrowth into a peripheral nerve graft. Vision Res 44: 2667–2674.
57. Tomita H, Sugano E, Yawo H, Ishizuka T, Isago H, et al. (2007) Restoration of visual response in aged dystrophic RCS rats using AAV-mediated channelopsin-2 gene transfer. Invest Ophthalmol Vis Sci 48: 3821–3826.
58. Tomita H, Sugano E, Isago H, Hiroi T, Wang Z, et al. (2010) Channelrhodopsin-2 gene transduced into retinal ganglion cells restores functional vision in genetically blind rats. Exp Eye Res 90: 429–436.
59. Tian N, Copenhagen DR (2003) Visual stimulation is required for refinement of ON and OFF pathways in postnatal retina. Neuron 39: 85–96.
60. Hannibal J, Fahrenkrug J (2004) Melanopsin containing retinal ganglion cells are light responsive from birth. Neuroreport 15: 2317–2320.
61. Misslin R, Cirang M (1986) Does neophobia necessarily imply fear or anxiety. Behavioural Processes 12: 45–50.
62. Berson DM, Castrucci AM, Provencio I (2010) Morphology and mosaics of melanopsin-expressing retinal ganglion cell types in mice. J Comp Neurol 518: 2405–2422.
63. Seeliger MW, Grimm C, Stahlberg F, Friedburg C, Jaissle G, et al. (2001) New views on RPE65 deficiency: the rod system is the source of vision in a mouse model of Leber congenital amaurosis. Nat Genet 29: 70–74.
64. Mojumder DK, Wensel TG (2010) Topical mydriatics affect light-evoked retinal responses in anesthetized mice. Invest Ophthalmol Vis Sci 51: 567–576.
65. Hubel DH, Wiesel TN (1962) Receptive fields, binocular interaction and functional architecture in the cat's visual cortex. J Physiol 160: 106–154.
66. MacLean P (1949) Psychosomatic disease and the visceral brain; recent developments bearing on the Papez theory of emotion. Psychosom Med 11: 338–353.
67. Papez J (1937) A proposed mechanism of emotion. Arch Neurol Psychiatry 38: 725–734.
68. Vann SD, Aggleton JP, Maguire EA (2009) What does the retrosplenial cortex do? Nat Rev Neurosci 10: 792–802.
69. Garcia Del Cano G, Gerrikagoitia I, Martinez-Millan L (2000) Morphology and topographical organization of the retrospleniocollicular connection: a pathway

to relay contextual information from the environment to the superior colliculus. J Comp Neurol 425: 393–408.
70. Wyss JM, Van Groen T (1992) Connections between the retrosplenial cortex and the hippocampal formation in the rat: a review. Hippocampus 2: 1–11.
71. Ochsner KN, Phelps E (2007) Emerging perspectives on emotion-cognition interactions. Trends Cogn Sci 11: 317–318.
72. Thiels E, Hoffman EK, Gorin MB (2008) A reliable behavioral assay for the assessment of sustained photophobia in mice. Curr Eye Res 33: 483–491.
73. Onaivi ES, Martin BR (1989) Neuropharmacological and physiological validation of a computer-controlled two-compartment black and white box for the assessment of anxiety. Prog Neuropsychopharmacol Biol Psychiatry 13: 963–976.
74. Vugler A, Carr AJ, Lawrence J, Chen LL, Burrell K, et al. (2008) Elucidating the phenomenon of HESC-derived RPE: anatomy of cell genesis, expansion and retinal transplantation. Exp Neurol 214: 347–361.
75. May CA, Lutjen-Drecoll E (2002) Morphology of the murine optic nerve. Invest Ophthalmol Vis Sci 43: 2206–2212.
76. Paxinos G, Franklin K (2001) The mouse brain in stereotaxic coordinates. San Diego.
77. Vugler AA, Coffey PJ (2003) Loss of calretinin immunoreactive fibers in subcortical visual recipient structures of the RCS dystrophic rat. Exp Neurol 184: 464–478.
78. Arai M, Arai R, Sasamoto K, Kani K, Maeda T, et al. (1993) Appearance of calretinin-immunoreactive neurons in the upper layers of the rat superior colliculus after eye enucleation. Brain Res 613: 341–346.
79. Gobersztejn F, Britto LR (1996) Calretinin in the mouse superior colliculus originates from retinal ganglion cells. Braz J Med Biol Res 29: 1507–1511.
80. Sugano E, Tomita H, Ishiguro S, Abe T, Tamai M (2005) Establishment of effective methods for transducing genes into iris pigment epithelial cells by using adeno-associated virus type 2. Invest Ophthalmol Vis Sci 46: 3341–3348.

Molecular Human Reproduction, Vol.16, No.7 pp. 441–451, 2010
Advanced Access publication on March 11, 2010 doi:10.1093/molehr/gaq007

MHR ORIGINAL RESEARCH

Intrinsic oxidative stress causes either 2-cell arrest or cell death depending on developmental stage of the embryos from SOD1-deficient mice

Naoko Kimura[1,*], Satoshi Tsunoda[2], Yoshihito Iuchi[2], Hiroyuki Abe[3], Kiyoshi Totsukawa[1], and Junichi Fujii[2]

[1]Laboratory of Animal Reproduction, Faculty of Agricultural Sciences, Yamagata University, Tsuruoka 997-8555, Japan [2]Department of Biochemistry and Molecular Biology, Graduate School of Medical Science, Yamagata University, Yamagata 990-9585, Japan [3]Graduate Program of Human Sensing and Functional Sensor Engineering, Graduate School of Science and Engineering, Yamagata University, Yonezawa 992-8510, Japan

*Correspondence address. Laboratory of Animal Reproduction, Faculty of Agricultural Sciences, Yamagata University, 1-23 Wakaba-machi, Tsuruoka 997-8555, Japan. Tel/Fax: +81-235-28-2871; E-mail: naonao@tds1.tr.yamagata-u.ac.jp

Submitted on June 18, 2009; resubmitted on January 19, 2010; accepted on January 26, 2010

ABSTRACT: Oxidative stress characterized by elevated reactive oxygen species is a well-known cause of developmental arrest and cellular fragmentation in the development of *in vitro*-produced embryos. To investigate the effects of intrinsic oxidative stress on the early development of embryos, oocytes from superoxide dismutase 1 (SOD1)-deficient mice resulting from *in vitro* fertilization, followed by culture for 4 days, were examined. Development of all embryos from SOD1-deficient oocytes was arrested at the 2-cell stage under conventional culture conditions with atmospheric oxygen (20% O_2). Significantly higher levels of superoxide were detected in SOD1-deficinet embryos cultured under 20% O_2 using dihydroethidium. Among treatments with antioxidants, only hypoxic culture with 1% O_2 negated the 2-cell arrest and advanced the development of the embryos with efficacy similar to that in wild-type embryos. Mitochondrial function was investigated because its malfunction was a suspected cause of 2-cell arrest. However, respiratory activity, ATP content and mitochondrial membrane potential in the 2-cell embryos were not markedly affected by culture with 20% O_2. When embryos from SOD1-deficient oocytes were first developed to the 4-cell stage under 1% O_2 culture and were then transferred to 20% O_2, most of them developed to the morula stage but underwent total degeneration thereafter. Thus, oxidative stress was found to damage embryos differentially, depending on the developmental stage. These results suggest that embryos derived from SOD1-deficient mouse oocytes are an ideal model to investigate intrinsic oxidative stress-induced developmental abnormality.

Key words: SOD1 deficiency / oxidative stress / 2-cell arrest / mitochondria

Introduction

It is universally accepted that mammalian preimplantation embryos are sensitive to their environment and that culture conditions, including collection and manipulation, have a momentous impact on the developmental potential of the embryos (Loutradis *et al.*, 2000; Summers and Biggers, 2003). *In vitro* fertilized (IVF) embryos in most mouse strains often show developmental arrest, e.g. 2-cell arrest or cellular fragmentation before the blastocyst stage, due to various deterioration factors during culture (Chatot *et al.*, 1990; Jurisicova and Acton, 2004). Among factors that have a deteriorating effect on fertilizability and subsequent developmental competence, oxidative stress, a condition with an overabundance of oxidants relative to antioxidants, is a well-known cause of developmental arrest, cell death by necrosis or by apoptosis, suppression of sperm motility and sperm–oocyte fusion (Noda *et al.*, 1991; Feugang *et al.*, 2004; Aitken and Baker, 2006). During culture under atmospheric conditions (approximately 20% O_2), embryos are exposed to a higher oxygen concentration than is physiologically normal in the oviduct and uterus (2% to 8% O_2; Fischer and Bavister, 1993). Elevated oxygen concentration advances the generation of cytotoxic reactive oxygen species (ROS), which can induce lipid peroxidation and functionally alter proteins and DNA (Nasr-Esfahani *et al.*, 1990; Takahashi *et al.*, 2000; Aitken and Baker, 2006). Hence, oxidative stress must be kept at a low level. Moreover, oxidative stress is augmented by various stimuli and maternal aging and exerts deteriorating effects on oocytes, consequently impairing reproductive ability (Fujii *et al.*, 2005; Agarwal *et al.*, 2008; Ruder *et al.*, 2008).

Transient metal ions, such as iron and copper, in the presence of superoxide and hydrogen peroxide, result in the generation of hydroxyl radicals, the most harmful reactive ROS, via the Fenton reaction (Halliwell and Gutteridge, 1999). The mechanism by which ethylenediamine tetraacetic acid (EDTA) supports embryo development *in vitro* (Suzuki *et al.*, 1988; Jinno *et al.*, 1989) is, at least in part, based on elimination of the free transition metal ions. ROS are also produced during the consumption of respired oxygen and other biological reactions involving reduction-oxidation reactions. In fact, the mitochondrial electron transfer system is a major source of ROS because it consumes more than 90% of the oxygen molecules respired by ordinary cells (Halliwell and Gutteridge, 1999).

The body has multiple antioxidative systems to suppress oxidative stress. Among the known antioxidative proteins, superoxide dismutase (SOD) is thought to play a central role because of its ability to scavenge superoxide anions, the primary ROS generated from molecular oxygen in cells, at the initial stage of the radical chain reaction (Fridovich, 1995). There are three kinds of mammalian SOD genes (Valentine *et al.*, 2005): the SOD1 product is localized in the cytosol and the intermembrane space of mitochondria; the SOD2 product is exclusively located in the mitochondrial matrix and the SOD3 product circulates in plasma. Regardless of the pivotal role of SOD1, SOD1-deficient mice show relatively mild phenotypes and grow normally (Ho *et al.*, 1998; Matzuk *et al.*, 1998), compared with mice lacking SOD2 protein, which die due to dilated cardiomyopathy during the neonatal stage (Li *et al.*, 1995). The prominent phenotype of SOD1-deficient mice is female infertility (Ho *et al.*, 1998; Matzuk *et al.*, 1998). Matzuk *et al.* (1998) have found a decrease in serum follicle stimulating hormone and luteinizing hormone levels and have proposed that ovary dysfunction may be secondary to decreased gonadotrophins and/or decreased responsiveness of the ovaries to physiological concentrations of gonadotrophins. On the other hand, Ho *et al.* (1998) showed that the number of 4 embryos in uteri of SOD1-deficient mice were not significantly different from those in wild-type mice and concluded that embryonic lethality was a cause of infertility. Thus, there are conflicting data, and it is yet unclear what actually causes female infertility in SOD1-deficient mice.

The authors are attempting to elucidate the underlying mechanism of female infertility in SOD1-deficient mice. This communication reports that intrinsic oxidative stress-injured embryos from SOD1-deficient mice respond differentially, in a development stage-specific manner.

Materials and Methods

Experimental animals

Three pairs of C57BL/6 *SOD1*$^{+/-}$ mice, originally established by Matzuk *et al.* (1998), were purchased through Jackson Laboratories (Bar Harbor, ME, USA) and bred at our institute, giving rise to *SOD1*$^{+/+}$ and *SOD1*$^{-/-}$ littermates. They were genotyped by PCR amplification as described previously (Iuchi *et al.*, 2007). Mice backcrossed to C57BL/6 mice more than eight times were used in this study. Four- to 6-week-old female mice were used to maximize the yield of oocytes in response to hormone stimulation, and 8- to 16-week-old male mice were used to collect epididymal spermatozoa. The animal room climate was kept under specific pathogen-free conditions at a constant temperature of 20–22°C with a 12-h alternating light–dark cycle, with food and water available *ad libitum*. Animal experiments were performed in accordance with the Declaration of Helsinki under the protocol approved by the Animal Research Committee of Yamagata University.

Oocyte collection, IVF and embryo culture

SOD1-deficient (*SOD1*$^{-/-}$) female mice and C57BL/6 background genetic controls (*SOD1*$^{+/+}$) were superovulated with 5 IU of equine chorionic gonadotrophin (Sankyo-elu, Tokyo, Japan), followed 48 h later with 5 IU of human chorionic gonadotrophin (Asuka-seiyaku, Tokyo, Japan) administered intra-peritoneally. Human tubal fluid (HTF) medium was used for IVF (Quinn *et al.*, 1985), and potassium simplex optimization medium (KSOM) was used for mouse oocytes/embryos cultures (Erbach *et al.*, 1994). For IVF, spermatozoa from *SOD1*$^{+/+}$ male mice were collected by squeezing the epididymal cauda and were pooled into a drop of HTF, supplemented with 0.5% bovine serum albumin (BSA fraction V, Sigma-Aldrich, St Louis, MO, USA). They were adjusted to a final concentration of $1-2 \times 10^6$ sperm/ml with the same medium and were then pre-incubated for 1 h. Ovulated cumulus–oocyte complexes (COCs) were collected by tearing the oviductal ampulla at 14–15 h after hCG injection and were pooled into the droplet with sperm. COCs were co-incubated with spermatozoa for 5 h. After IVF, presumptive zygotes were stripped of cumulus and sperm cells in KSOM supplemented with 0.5% BSA for embryo culture. Cleavage rates were assessed at 24 h after the start of embryo culture. Normally cleaved embryos remained in culture for 4 days (up to the blastocyst stage).

Each culture was kept in 200 μl droplets (groups of 10–20 oocytes/embryos) of medium overlaid with mineral oil in plastic dishes. Incubation was conducted at 37°C under a humidified atmosphere of either 20% O_2 (5% CO_2 in air) or 1% O_2 (1% O_2/5% CO_2/94% N_2). The effects of antioxidants, culturing under supplementation with 100 μM β-mercaptoethanol (Wako Pure Chemical Industries, Osaka, Japan) or 500 μg/ml human SOD1 protein, on fertilization and embryo development were also investigated in normoxic conditions.

Western blot analysis

To detect SOD1 and SOD2 protein expression, ovulated COCs derived from each genotype (*SOD1*$^{-/-}$, *SOD1*$^{+/-}$, *SOD1*$^{+/+}$) of mice were denuded by hyaluronidase treatment (300 μg/ml in KSOM, type IVs, Sigma-Aldrich) and presumptive metaphase II (M II) oocytes with the first polar body were collected. Each genotype sample of 60 oocytes was washed in PBS containing 3 mg/ml polyvinylalcohol (PVA, Sigma-Aldrich), sonicated for 1 s, and then lysed in 2% SDS and 60 mM Tris–HCl-based sampling buffer (pH 6.8). The lysates were separated by electrophoresis in 15% SDS–PAGE and electrically transferred onto PVDF membranes (Millipore, Billerica, MA, USA). After blocking with 5% (w/v) skim milk in 0.1% (v/v) Tween-20-tris-buffered saline (T-TBS) for 1 h, the membrane was incubated overnight at 4°C with a goat antihuman SOD1 polyclonal antibody (Ishii *et al.*, 2005) diluted 1:1000 in Can Get Signal® solution I (Toyobo, Oosaka, Japan). Following three washes of 5 min each in T-TBS, the membrane was incubated for 1 h at room temperature with a horseradish peroxidase (HRP)-conjugated anti-goat second antibody (Zymed Laboratories, South San Francisco, CA, USA) diluted 1:20 000 in Can Get Signal® solution II. After three washes in T-TBS, the blots were visualized using an ECL detection kit (Amersham Pharmacia Biosciences, Piscataway, NJ, USA). The membrane was then incubated for 30 m at 50°C in stripping buffer (2% SDS, 100 μM β-mercaptoethanol and 60 mM Tris–HCl) to remove the antibodies. In the same manner described above, SOD2 (Suzuki *et al.*, 1993) and glyceraldehydes-3-phosphate dehydrogenase (G3PDH, Santa Cruz Biotechnology, Santa Cruz, CA, USA) proteins were detected by rabbit antihuman SOD2 polyclonal antibody diluted 1:1200 or by rabbit antihuman

G3PDH diluted 1:1000, as the first antibody, and HRP-conjugated anti-rabbit diluted 1:40 000, as the second antibody.

Chromosome labeling of zygotes/embryos

To successively compare the transition from zygote to 2-cell stage embryo in SOD1-deficient mice and wild-type mice, at 5, 18, 20, 36 and 42 h after IVF under 20% O_2, the zygotes/embryos were fixed with 2% formaldehyde in PBS-PVA for 30 min and stained with 10 μg/ml Hoechst33342 (Sigma-Aldrich) in PBS-PVA for 15 min at room temperature. After three washes in PBS-PVA, the embryos were observed under a fluorescence microscope (Olympus, Tokyo, Japan).

Detection of superoxide in 2-cell stage embryos

The level of intracellular superoxide in 2-cell stage embryo was determined using dihydroethidium (Molecular Probes, Eugene, OR, USA), a specific indicator of superoxide. At 36 h after IVF, the embryos were incubated with 2.5 μM dihydroethidium in KSOM for 10 min at 37°C in the dark, then washed and continuously cultured in KSOM for 30 min. Superoxide-specific fluorescence was detected using a fluorescent microscope (Leica DMI3000B, Leica Microsystems, Wetzlar, Germany) at fluorescence maximum 515/590 nm (excitation/emission). An image was obtained for the optical section of each embryo when two divided cells lined a plane. Individual images were analyzed using Image J software ver.1.38 (developed by NIH), which allows for quantification of signal intensity of dihydroethidium staining. Signal intensity was expressed by the integration of average pixels in each embryo. Relative values of signal intensity were calculated by the mean value of a wild-type embryo to the individual value of wild-type or SOD1-deficient embryos under the same oxygen conditions.

Respiration assay of 2-cell stage embryos

At 36 h after IVF, the oxygen consumption of individual 2-cell embryos was quantified non-invasively by a modified scanning electrochemical microscope (SECM) measuring system (Shiku *et al.*, 2001; Abe, 2007). The oxygen consumption of the embryos was indicated by the oxygen concentration difference between the bulk solution and the sample surface, using voltammetry of the Pt-microdisc electrode (Shiku *et al.*, 2004). The tip potential was held at −0.6 V versus Ag/AgCl with a potentiostat to monitor the local oxygen concentration in the solution. Modified HTF medium was employed for the measurement of oxygen consumption. Its composition includes only salt electrolyte, glucose, sodium pyruvate, sodium lactate, HEPES and gentamicin sulfate. Voltammetry of the Pt-microdisc electrode in the modified HTF medium showed a steady-state oxygen reduction wave. No response from other electrochemically active species was observed near the embryo surface. The single embryo was transferred into a cone-shaped microwell filled with modified HTF medium at 37°C on a warming plate (MATS502NLR; Tokai Hit, Shizuoka, Japan) where it fell to the bottom of the well and remained at the lowest point. The microelectrode was scanned according to the *z*-direction from the side point of the sample. The motor-driven XYZ stage was located on the microscope stage for electrode tip scanning. The XYZ stage and potentiostat were controlled by a computer. The oxygen consumption rate of each embryo was calculated by software based on the spherical diffusion theory (Shiku *et al.*, 2004). Each embryo was scanned three times.

Measurement of ATP content of 2-cell stage embryos

At 36 h after IVF, the ATP content of individual embryos was measured using a commercial assay based on the luciferin–luciferase reaction, using a BacTiter-GloTM Microbial Cell Viability Assay Kit (Promega, Madison, WI, USA). Briefly, samples were rinsed three times in PBS-PVA, suspended in 50 μl PBS, and stored at −80°C until use. After the addition of a 50-μl reaction mixture followed by incubation at 25°C for 5 min, chemiluminescence of the sample was measured by a luminometer (Berthold Lumat LB9507, Bad Wildbad, Germany). A 5-point standard curve (0–100 pmol/tube) was routinely included in each assay. The ATP content was determined from the formula for a standard curve (linear regression). The linear relationship was observed between luciferin luminescence and ATP content from a 0.01–10 pmol/assay, which fully covered ATP contents in each embryo.

Measurement of mitochondrial membrane potential in 2-cell stage embryos

Mitochondrial membrane potential ($\Delta\Psi m$) was determined by staining 2-cell stage embryos with the mitochondrial stain JC-1 (5,5′,6,6′-tetrachloro-1,1′,3,3′-tetraethylbenzimidazolyl carbocyanine iodide, Mitochondrial Membrane Potential Assay Kit, Cayman Chemical Company, Ann Arbor, MI, USA). At 36 h after IVF under 20% O_2, the embryos were incubated in JC-1 at half the manufacturer's recommended concentration (1:200 in KSOM) for 15 min at 37°C in the dark, then washed and immediately examined using a fluorescent microscope (Leica DMI3000B, Leica Microsystems). One optical section was imaged for each embryo, in the plane where both cleaved cells could be visualized. Individual images of fluorescently labeled embryos were analyzed using Image J software ver.1.38 (developed by NIH), which allows for quantification of signal intensity of JC-1 staining. $\Delta\Psi m$ was estimated by the representing integration of average red pixels (J-aggregate, high membrane potential) as a ratio of average green pixels (J-monomer, low membrane potential) in the same area for each embryo.

Analysis of degenerated embryos

To characterize cellular damage, at Day 4 after IVF, embryos were reacted with 10 μg/ml Hoechst33 342, 5 μg/ml propidium iodide (PI) or FITC-labeled annexin V using a MEBCYTO® Apoptosis Kit (Medical and Biological Laboratories, Woburn, MA, USA) and 5 μg/ml Hoechst33342 for 15 min at room temperature. After washing three times with PBS-PVA, samples were examined with a fluorescent microscope (Leica DMI3000B, Leica Microsystems).

Statistical analysis

Data showing embryo development in normoxic and hypoxic culture consist of at least three independent replicates. A Fisher's exact test was performed to evaluate the developmental ability among individual groups. Statistical analyses of signal intensity by dihydroethidium staining or JC-1 staining, respiration assay and ATP content were carried out using the Bonferroni test. A *P*-value of <0.05 was considered statistically significant.

Results

Two-cell arrest of embryos from SOD1-deficient mouse oocytes and rescue under hypoxic culture

Western blot analysis indicated that SOD1 protein was present in oocytes from wild- and hetero-type mice, but was totally absent in oocytes from SOD1-deficient mice, whereas a similar amount of SOD2 protein was present in both (Fig. 1). The developmental ability of fertilized oocytes from SOD1-deficient mice after IVF was

examined in comparison with wild-type mice (Table I). When oocytes from wild-type mice were fertilized with sperm from wild-type mice, the fertilized oocytes developed into blastocysts with normal frequency in 4 days. On the other hand, development of the fertilized oocytes from SOD1-deficient mice was totally arrested at the 2-cell stage. The zygotes/embryos from SOD1-deficient mice were examined by DNA labeling with Hoechst33342 from 5 to 42 h after IVF. No abnormality was observed in the timing of pro-nucleus formation and the first cleavage of SOD1-deficient zygotes/embryos, compared with wild-type zygotes/embryos (Fig. 2). Because SOD1 protein rescues the 2-cell arrest that occurs in embryos of some mouse strains (Nonogaki *et al.*, 1992), the effects of antioxidants, human SOD1 protein and β-mercaptoethanol on IVF and further development were examined, but 2-cell arrest was not negated in any of the embryos from SOD-deficient oocytes. Thus, oxidative stress caused by SOD1 deficiency appeared to be different from that in previously reported cases.

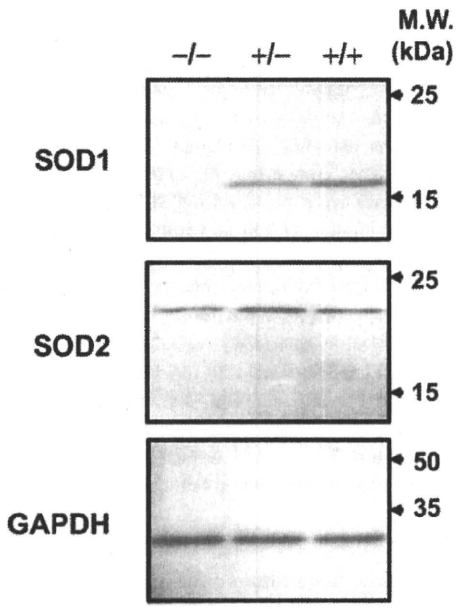

Figure 1 Western blot analysis of SOD1 and SOD2 in oocytes. Sixty superovulated MII oocytes from each genotypic female mouse were subjected to SDS–PAGE followed by immunoblot analysis. Antibodies against SOD1 (upper panel), SOD2 (middle panel) and GAPDH (lower panel, protein loading control) were used as primary antibodies.

Since oxygen content is ~2% in the body, which is one order lower than the conventional culture conditions with atmospheric oxygen (20% O_2, 150 mmHg), culture was attempted under hypoxic conditions with 1% O_2 (7 mmHg). As expected, embryos from SOD1-deficient mice developed beyond the 2-cell stage to blastocyst with efficacy comparable to those from wild-type mice (Table I). Thus, SOD1-deficient oocytes were found to be vulnerable to exposure to atmospheric oxygen conditions, but developed normally under hypoxic culture.

Higher concentration of superoxide in 2-cell arrest embryos

We estimated the oxidative stress in 2-cell embryos from wild-type and SOD1-deficient oocytes at 36 h after IVF using dihydroethidium, which is a fluorescent probe frequently used to measure intracellular superoxide levels (Wilhelm *et al.*, 2009). The resultant fluorescence was detected spottily in the cytoplasm of both wild-type and SOD1-deficient embryos under 20% O_2 (Fig. 3A). Then we quantified fluorescence intensity of all four groups of embryos. The data indicated that superoxide levels in SOD1-deficient embryos were significantly higher than that in the embryos from wild-type embryo under 20% O_2 (Fig. 3B). However, there was no significant difference between wild-type and SOD1-deficient embryos under 1% O_2 culture.

Embryos gradually changed to permanent 2-cell arrest under atmospheric oxygen

To determine the period required for the arrest, the embryos were incubated under atmospheric oxygen conditions for 12, 24 and 36 h after IVF, transferred to 1% O_2 and incubated up to 4 days (Fig. 4). There was no important effect of atmospheric culture on the

Table I Developmental arrest at 2-cell stage in embryos derived from SOD1-deficient (KO) mouse oocytes under 20% or 1% oxygen culture and effects of antioxidant supplementations.

Oocyte genotype and treatments	Number of oocytes cultured	Number of embryos (%)		
		2-cell ≤ at Day 1	4-cell ≤ at Day 2	Blastocyst at Day 4
Under 20% O_2				
Wild	89	85 (95.5)[a]	83 (93.3)[a]	75 (84.3)[a]
KO	76	72 (94.7)[a]	0 (0)[b]	0 (0)[c]
KO + 100 μM β-mercapotethanol	95	61 (64.2)[c]	0 (0)[c]	0 (0)[c]
KO + 500 μg/ml hSOD1	91	73 (80.2)[b]	0 (0)[c]	0 (0)[c]
Under 1% O_2				
Wild	79	77 (97.5)[a]	68 (86.1)[a]	53 (67.1)[b]
KO	96	93 (96.9)[a]	81 (84.4)[a]	59 (61.5)[b]

WT, wild-type. Values with difference superscript letters within each day are significantly different ($P < 0.05$).

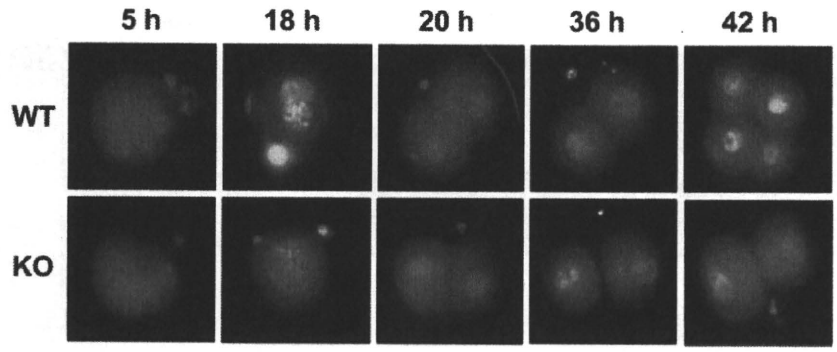

Figure 2 Chromosome labeling of zygotes/embryos. Superovulated COCs from wild-type (WT) or SOD1-deficient (KO) mice were subjected to IVF and incubated under atmospheric oxygen conditions. The zygotes/embryos were stained with Hoechst33342 at 5, 18, 20, 36 and 42 h after IVF and observed under a fluorescent microscope.

development of embryos from SOD1-deficient oocytes by 12 h. However, the developmental potential of the 4-cell and blastocyst stages in SOD1-deficient embryos decreased gradually during the 2-day incubation under atmospheric oxygen. The hypoxic culture did not rescue most embryos with 2-cell arrest after 36 h incubation under atmospheric oxygen (4-cell: 12.7%, blastocyst: 3.6%). This was regarded as permanent embryo arrest, with characteristics similar to the 2-cell arrest observed in embryos from ordinary mice (Betts and Madan, 2008).

No changes in mitochondrial membrane potential and mitochondrial function in 2-cell arrested embryos

Mitochondrial function was also examined by measuring the respiration and ATP content of individual 2-cell embryos. Respiratory activity, as judged by oxygen consumption in a single embryo using the SECM measuring system, did not differ significantly between the embryos from wild-type and SOD1-deficient mouse oocytes at 36 h after IVF (Fig. 5A). Measurement of ATP content again showed no significant difference between embryos from the two genotypes under 1% and 20% O_2 cultures (Fig. 5B). Taken together, these data indicate that mitochondria were normal in embryos that were derived from the SOD1-deficient mouse oocytes and arrested at the 2-cell stage by incubation under 20% O_2. Since mitochondria are major organelles that produce ROS, and their malfunction is a proposed cause of 2-cell arrest (Liu *et al.*, 2000; Thouas *et al.*, 2004), we assessed $\Delta\Psi$m using cationic dye, JC-1, which is an important parameter of mitochondria function and has been used as an indicator of cell activity. At 36 h after IVF, putative J-aggregate fluorescence was thickly detected in the peri-cortical cytoplasm of the 2-cell stage embryos, and J-monomer fluorescence was distinctly detected in the peri-nuclear region. There was no difference in the distribution of both J-aggregate and J-monomer fluorescence between the two groups (Fig. 6A). The $\Delta\Psi$m ratio of J-aggregate to J-monomer in SOD1-deficient embryos seemed to be slightly higher than that in the embryos from wild-type, but no prominent difference existed between the two groups (Fig. 6B).

Differential injury of zygotes versus 4-cell embryos from SOD1-deficient mouse oocytes by atmospheric culture

The question of whether oxygen toxicity was found only at the 2-cell stage was then examined. First the embryos were developed to the 4-cell stage by incubation under hypoxic conditions for 42 h after IVF, then transferred to atmospheric oxygen conditions and incubated further. The 4-cell embryos from SOD1-deficient mouse oocytes developed to the morula stage, but could not develop into blastocysts (Table II). Since cellular degeneration was evident in embryos from SOD1-deficient mouse oocytes, the impaired embryos were further characterized by reaction with FITC-annexin V, Hoechst33 342 and PI. FITC-annexin V strongly stained the embryos from SOD1-deficient mouse oocytes (Fig. 7, 2a–2f), but only minimally stained the embryos from wild-type mouse oocytes (Fig. 7, 1a–1f). Staining with Hoechst33 342, which detects nuclear DNA in any cell, and PI, which detects only the nuclear DNA of cells with leaky membranes, indicated nuclear fragmentation in degenerated embryos from SOD1-deficient mouse oocytes. Some FITC-annexin V positive cells were stained with Hoechst33 342 but not with PI, which is consistent with apoptotic cell death. Thus, the 4-cell embryos from SOD1-deficient mouse oocytes that overcame 2-cell arrest were more severely damaged than 1-cell embryos (zygotes) by oxidative stress.

Discussion

Developmental arrest in *in vitro*-produced embryos is commonly observed in several strains of mice and other species (Betts and Madan, 2008). Among a variety of factors that cause such arrest, oxygen deteriorates the development of the 2-cell mouse embryo (Auerbach and Brinster, 1968). Oxidative stress due to elevated ROS is a likely cause of 2-cell arrest and has been extensively studied in relation to the quality of oocytes (Noda *et al.*, 1991; Tarin, 1996). In the case of developing human embryos, EDTA effectively supports embryonic development (Suzuki *et al.*, 1988; Jinno *et al.*, 1989). It plays the role of an antioxidant by chelating transition metal ions, which cause production of a hydroxyl radical via the

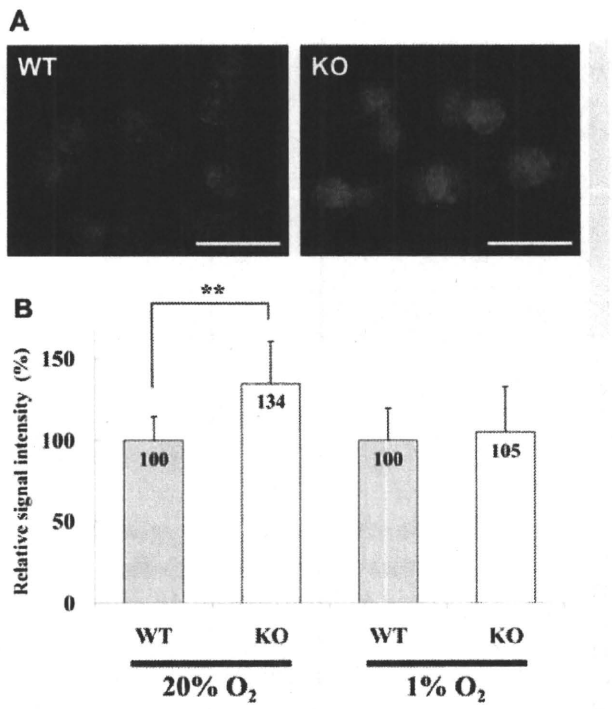

Figure 3 Fluorescent images and signal intensity of 2-cell embryos stained with dihydroethidium. (**A**) Two-cell embryos from wild-type (WT) or SOD1-deficient (KO) mouse oocytes under 20% O_2 after dihydroethidium staining. Scale bars, 100 μm. (**B**) Embryos from wild-type (WT) and SOD1-deficient (KO) oocytes were cultured under 1% or 20% O_2 for 36 h after IVF. Then, superoxide in the individual 2-cell embryos was detected by dihydroethidium staining ($n = 14–17$). Signal intensity was shown as a relative value of averaged WT value into individual WT value or KO value in the same culture condition. Bars represent the mean ± SD of individual embryos. Differences were considered to be significant when $^{**}P < 0.01$. The numbers inside bars indicate the mean value.

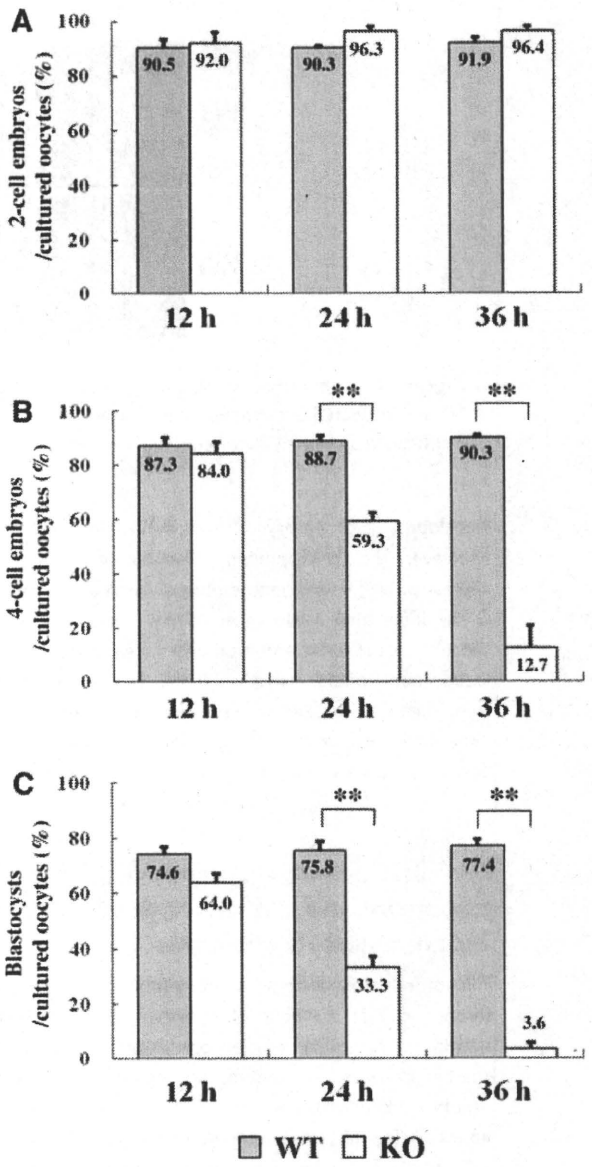

Figure 4 Time required for 2-cell arrest in oocytes from SOD1-deficient mice. Superovulated COCs from wild-type or SOD1-deficient mice were subjected to *in vitro* fertilization (IVF) and incubated under atmospheric oxygen conditions, and then transferred to 1% O_2 at 12, 24 and 36 h after IVF. (**A**) Fertilized oocytes were assessed as 2-cell embryos at 24 h after IVF. (**B**) The number of 4-cell embryos was counted at 48 h after IVF. (**C**) The number of blastocysts was counted after 4 days culture. Within each graph, the numbers inside the bars indicate the mean value. Numbers of each group embryo examined were 12 h-WT, $n = 63$; 12 h-KO, $n = 50$; 24 h-WT, $n = 62$; 24 h-KO, $n = 54$; 36 h-WT, $n = 62$; 12 h-KO, $n = 55$. Differences were considered to be significant when $^{**}P < 0.01$.

Fenton reaction. Experimental results provide direct evidence that supplementation of SOD protein and thioredoxin in the culture medium negates the arrest (Goto *et al.*, 1992; Nonogaki *et al.*, 1992). In this study, total 2-cell arrest was observed in embryos from SOD1-deficient mice oocytes under culture with atmospheric oxygen, but supplementation of SOD1 protein or β-mercaptoethanol was found to be ineffective (Table 1).

In most studies regarding oxidative stress on embryonic development, hydrogen peroxides and other (pro) oxidants have been used to trigger oxidative stress extrinsically to embryos, and mitochondrial impairment has been observed (Liu *et al.*, 2000; Thouas *et al.*, 2004). In our study, a higher level of production for superoxide was detected in the prospective 2-cell arrest embryos from SOD1-deficient oocytes at 36 h after IVF, by dihydroethidium staining, suggesting that the 2-cell arrest was attributed to intrinsic oxidative stress caused by elevated superoxide due to SOD1 deficiency. Oocyte mitochondria consume ~50–70% of respired oxygen (Benos and Balaban, 1980), which is much less than most somatic cells, which consume more than 90%. Oxygenase present in oocytes consumes a portion of the remaining 20–30% oxygen (Balling *et al.*, 1985) and may be involved in superoxide production in the 2-cell embryos. Transient elevation of hydrogen peroxide, a

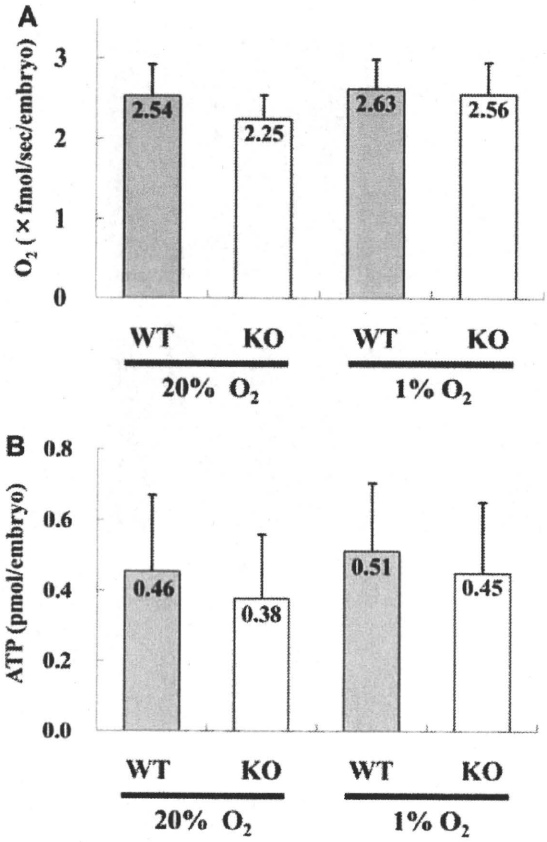

Figure 5 Respiratory activity and ATP levels of 2-cell embryos. (**A**) Embryos from wild-type (WT) or SOD1-deficient (KO) mouse oocytes were cultured under 1% or 20% O_2 for 36 h after IVF, and oxygen consumption in the individual embryos was measured by an SECM measuring system ($n = 10–13$). (**B**) ATP content in the individual embryos treated under the same conditions as (A) was measured ($n = 22–25$). Within each graph, bars represent the mean ± SD of individual embryos. The numbers inside the bars indicate the mean value.

dismutation product of superoxide, is shown in mouse 2-cell stage embryos when developmental arrest occurs (Nasr-Esfahani *et al.*, 1990). In addition, immaturity of the mitochondrial electron transport system may also be responsible for ROS production. Although oxygen consumption remains relatively constant from the zygotes to the morula before increasing dramatically at the blastocyst stage (Houghton *et al.*, 1996; Thompson *et al.*, 1996), mitochondria remain immature in oocytes and early embryos (Van Blerkom, 2004). This immaturity of the mitochondrial electron transfer system would cause inappropriate electron transfer to molecular oxygen instead of cytochrome c oxidase (complex IV), and result in the production of superoxide. Superoxide originating from these sources would remain high in SOD1-deficient embryos, resulting in oxidative stress that consequently causes 2-cell arrest. Because superoxide itself is not very reactive, how the elevated superoxide causes 2-cell arrest is unclear. Although nitric oxide (NO) plays a pivotal role in oocyte activation at fertilization and also in embryogenesis (Kuo *et al.*, 2000; Nishikimi *et al.*, 2001; Tranguch *et al.*, 2003), superoxide reacts rapidly with NO to generate peroxynitrite, which is a highly reactive molecule and oxidizes lipids, proteins and nucleic acids. Thus, elevation of superoxide due to SOD1 deficiency would eliminate the important signaling molecule NO and convert it to the harmful oxidant peroxynitrite.

Mitochondria lack histone and possess weak DNA-repairing ability, which makes mitochondrial DNA vulnerable to oxidative modification. In *in vivo* studies, aging increases oxidative damage in mitochondria, and the incidence of mitochondrial DNA mutations increases in human ovarian tissues after the age of 45 (Kitagawa *et al.*, 1993) and in fertilized oocytes collected from IVF patients at ages above 38 (Keefe *et al.*, 1995). Morphological abnormalities in oocyte mitochondria from old mice were also observed (Tarin *et al.*, 2001); thus, mitochondrial damage by ROS produced over long periods may be a mechanism leading to age-related decline in oocyte quality and chromosome aneuploidy (Tarin, 1996; Tarin *et al.*, 1998, 2000), as further supported by *in vitro* studies. Treatment of mouse zygotes with 200 μM hydrogen peroxide for 15 min causes a decline in mitochondrial membrane potential and mitochondrial malfunction (Liu *et al.*, 2000). Since developmental arrest occurs after this treatment, it can be concluded that mitochondrial malfunction contributes to cell-cycle arrest. Similar results are obtained when oxidation of mitochondria is induced by photosensitization using mitochondria-specific sensitizing dye (Thouas *et al.*, 2004). In many studies in which oxidative stress is induced by extracellularly administered ROS or prooxidants, the abnormal development of embryos is attributed to energy depletion by mitochondrial malfunction or induction of apoptosis by cytochrome c released from mitochondria. Low mitochondrial ATP content has been correlated with reduced developmental competence and post-implantation outcomes (Van Blerkom *et al.*, 1995). In the present study, respiratory activity, ATP content and $\Delta\Psi m$ of 2-cell embryos were examined at 36 h after IVF because embryos from wild-type mouse oocytes, regarded as the control embryos, developed further after 36 h. Most of the SOD1-deficient embryos incubated under 20% O_2 for 36 h were unable to develop further (Fig. 2), which indicated that this developmental arrest arose during 36 h incubation under 20% O_2. However, there was no evident difference in mitochondrial function between the wild-type embryos and the 2-cell arrested embryos from SOD1-deficient mouse oocytes at 36 h after IVF (Figs 5 and 6). Acton *et al.* (2004) showed that $\Delta\Psi m$ tend to increase slightly in the complete 2-cell arrest embryos at 68 h post-hCG compared with that in normal 2-cell embryos at 44 h post-hCG, when ICR zygotes were cultured in HTF. Taken together, these data on SOD1-deficient embryos suggest that mitochondrial malfunction may not play a major role in the developmental arrest of SOD1-deficient embryos. Trimarchi *et al.* (2000) have examined oxygen consumption of individual embryos and have shown that healthy embryos consume more oxygen than those undergoing cell death. On the basis of their criteria, the 2-cell embryos obtained from SOD1-deficient mice under hypoxic and atmospheric oxygen culture can be considered healthy. Therefore, we concluded that the 2-cell arrest observed in SOD1-deficient embryos is not due to either a defective energy supply or to cell death by mitochondrial malfunction.

The mechanism that causes 2-cell arrest of developing embryos from SOD1-deficient mice is yet unclear. It was observed that

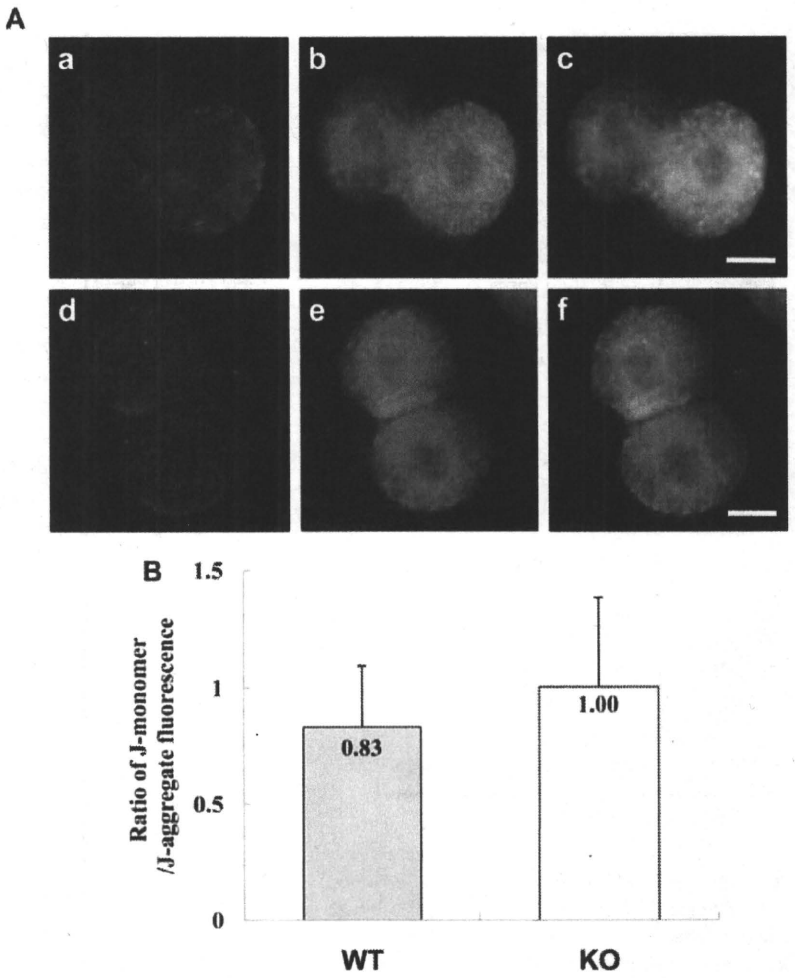

Figure 6 Fluorescent images and mitochondrial membrane potential of 2-cell embryos stained with JC-1. (**A**) Fluorescent images of JC-1-stained 2-cell embryos from wild-type (a–c) or SOD1-deficient (d–f) mouse oocytes under 20% O_2. (a and d) J-aggregate; (b and e) J-monomer; (c and f) Merge. Scale bars, 20 μm. (**B**) The ratio of J-aggregate to J-monomer fluorescence for individual embryo using JC-1 staining in embryos from wild-type (WT) or SOD1-deficient (KO) mouse oocytes cultured under 20% O_2 for 36 h after IVF ($n = 15–20$). Bars represent the mean ± SD of individual embryos. The numbers inside the bars indicate the mean value.

Table II Effect of converted culture from 1% to 20% oxygen on the development of 4-cell embryos from SOD1-deficient (KO) mouse oocytes.

Oocyte genotype	Number of oocytes cultured	Number of embryos (%)			
		2-cell ≤ at Day 1	4-cell ≤ at Day 2	Morula ≤ at Day 3	Blastocyst at Day 4
WT	54	50 (92.6)	48 (88.9)	44 (81.5)	39 (72.2)
KO	59	56 (94.9)	55 (93.2)	39 (66.1)	0 (0)**

WT, wild-type. Differences within each day were significant when $^{**}P < 0.01$.

embryonic cells were alive but permanently arrested, resembling cellular senescence. Knockdown of SOD1 by employing small interfering RNA actually induced senescence in human fibroblasts (Blander *et al.*, 2003). Regarding mouse embryos, defective $p34^{cdc2}$ kinase, a key regulator of the cell cycle, in 2-cell arrest and its restoration by SOD and thioredoxin, has been reported (Natsuyama *et al.*, 1993). Moreover, M-phase promoting factor and mitogen-activated protein kinase, whose activation constitutes a mitotic signal pathway, are

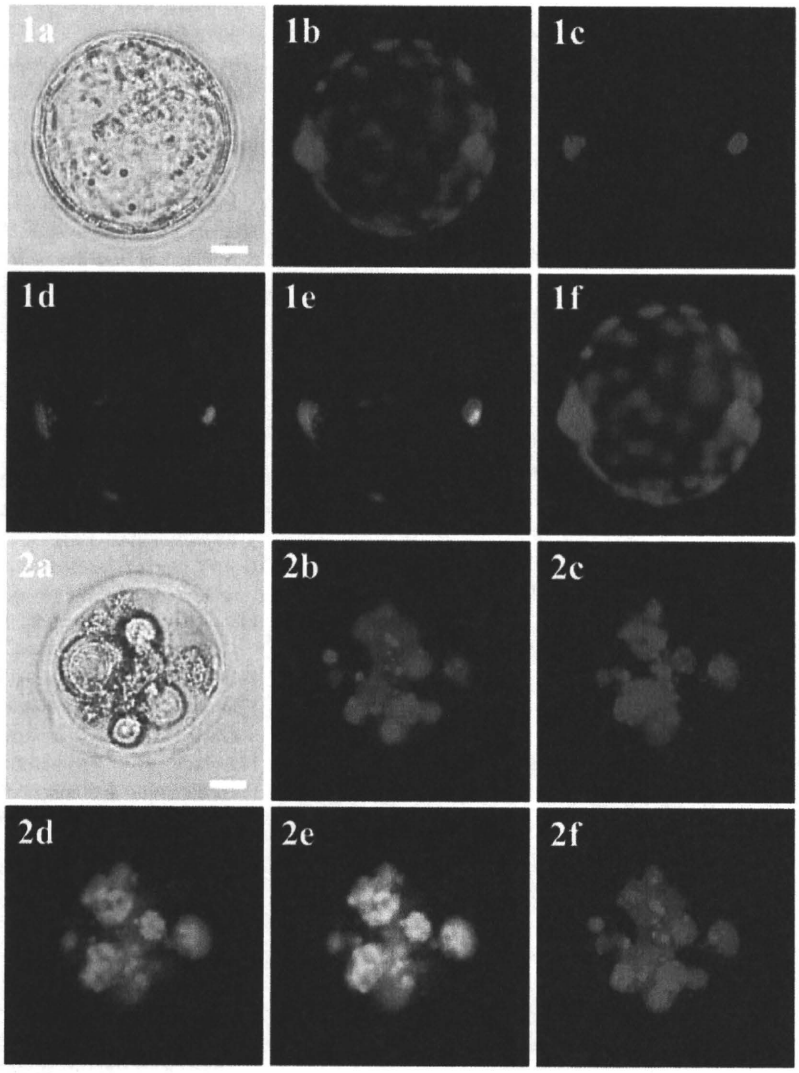

Figure 7 Cytological examination of embryos with abnormality. Superovulated COCs from wild-type mice (1a–1f) or SOD1-deficient mice (2a–2f) were subjected to IVF and incubated for 42 h after IVF under 1% O_2. Four-cell embryos were then transferred to atmospheric oxygen conditions and incubated further. At 4 days after IVF, embryos were stained with Hoechst 33342 (1b and 2b), PI (1c and 2c) and FITC-annexin V (1d and 2d) and were observed under a fluorescent microscope. Merged pictures between PI + FITC-annexin V (1e and 2e) and Hoechst33342 + PI (1f and 2f) are also shown. Scale bars, 20 μm.

down-regulated in oocytes ovulated from aged mice (Tatone *et al.*, 2006). On the other hand, the involvement of $p66^{Shc}$, a protein belonging to the Shc family of adaptors for signal transduction in mitogenic and apoptotic responses, in permanent embryo arrest in bovines has been proposed as a cause of oxidative stress (Favetta *et al.*, 2007; Betts and Madan, 2008). If this is the case, expression of a responsible gene(s) is essential to arrest the cell cycle. From this viewpoint, the stage of developmental arrest corresponds to the point when zygotic gene activation occurs in mouse embryos at the late 1- to 2-cell stages (Telford *et al.*, 1990; Schultz, 1993). When embryos from SOD1-deficient oocytes were developed to four cells under 1% O_2 and transferred to 20% O_2, embryos developed to the morula stage but degenerated thereafter (Table II, Fig. 7). In our preliminary experiment, when *in vivo*-developed 2-cell embryos were collected from SOD1-deficient oocytes and cultured for 3 days under 20% O_2, most of the embryos (24 of 26 embryos) arrested at the 3- to 4-cell stage. These results indicate that (i) the developmental arrest of SOD1-deficient embryos was caused by oxidative stress around the 2-cell stage regardless of IVF or *in vivo* fertilization and (ii) the oxygen exerted deteriorating effects on embryos in a different manner, depending on the developmental stage. Impaired regulation of the cell cycle would be responsible for 2-cell arrest by oxidative stress, while a mechanism for apoptosis appears to be involved in the degeneration of SOD1-deficient embryos at a later stage. Since mitochondria play pivotal roles in the initiation of apoptosis, the mitochondrial maturation process may be involved in the